Journal of Hazardous Materials 405 (2021) 123735

Contents lists available at ScienceDirect

Journal of Hazardous Materials

journal homepage: www.elsevier.com/locate/jhazmat

Treatment of waste gas contaminated with dichloromethane using photocatalytic oxidation, biodegradation and their combinations

Fares Almomani [a,*], Eldon R. Rene [b,c], María C. Veiga [b], Rahul R. Bhosale [a], Christian Kennes [b]

[a] Department of Chemical Engineering, College of Engineering, Qatar University, P. O. Box 2713, Doha, Qatar
[b] Chemical Engineering Laboratory, Faculty of Sciences and Center for Advanced Scientific Research (CICA), University of La Coruña (UDC), E-15008, La Coruña, Spain
[c] IHE Delft Institute for Water Education, Department of Water Supply, Sanitation and Environmental Engineering, P. O. Box 3015, 2601 DA, Delft, the Netherlands

ARTICLE INFO

Editor: G. Lyberatos

Keywords:
Dichloromethane
Air pollution
Hydroxyl radicals
Photo-degradation
Stirred tank bioreactor
Process optimization

ABSTRACT

The treatment of waste gas (WG) containing dichloromethane (DCM) using advanced oxidation processes (AOPs) [UV and UV-TiO_2], biological treatment (BT), and their combination (AOPs-BT) was tested. AOP tests were performed in an annular photo-reactor (APHR), while BT was conducted in a continuous stirred tank bioreactor (CSTBR). The effects of gas flow rate (Q_{gas}), inlet DCM concentration ($[DCM]_i$), residence time (τ), photocatalyst loading (PH-C_L) and % relative humidity (% RH) on the AOPs performance and the removal of DCM (%DCM_r) were studied and optimized. The UV process exhibited %$DCM_r \leq 12.5$ % for tests conducted at a $[DCM]_i \leq 0.45$ g/m^3, Q_{gas} of 0.12 m^3/h and τ of 27.6 s, respectively, and < 4 % when the $[DCM]_i \geq 4.2$ g/m^3. The UV-TiO_2 achieved a %$DCM_r \geq 71 \pm 1.5$ % at Q_{gas} of 0.06 m^3/h, $[DCM]_i$ of 0.45 g/m^3, τ of 55.2 s, PH-C_L of 10 g/m^2, and % RH of 50, respectively. The BT process removed ~97.6 % of DCM with an elimination capacity (EC) of 234.0 g/m^3·h. Besides, the high %DCM_r of ~98.5 % in the UV-BT and 99.7 % in the UV-TiO_2-BT processes confirms AOPs-BT as a promising technology for the treatment of recalcitrant compounds present in WG.

1. Introduction

Volatile organic compounds (VOCs) are present in industrial waste gases (IWGs) and it has a direct impact on human health and the environment (Beauchet et al., 2007; Chen et al., 2016; Chlala et al., 2016; Kasperczyk et al., 2019; Zhong et al., 2017). A major part of the VOCs contribute indirectly to the greenhouse gas effect, thereby causing the following problems: (1) global warming, (2) the formation of ground-level ozone (3) destroying stratospheric ozone, and (4) the formation of photochemical smog (Bravo et al., 2017; Hein et al., 2018; Al Momani, 2007a). Health problems including sensory irritation symptoms, allergies, asthma, neurological and liver toxicity, and cancer were related to the exposure and inhalation of VOCs (Matějová et al., 2013). Dichloromethane (DCM; CH_2Cl_2) was listed by the United States Environmental Protection Agency (US EPA) and the European Environment Agency (EEA) as an extremely dangerous and toxic waste gas (WG) with a high environmental risk that requires well-organized treatment and control technologies (Directive, 2013; Ribeiro et al., 2015). The emission of DCM to the atmosphere increased from 101 Gg/yr to 318 Gg/yr between the period 2005 and 2016 (Feng et al., 2018; Keppler et al., 2019). DCM is regularly used in various industries including aerosol paint, urethane, plastic manufacturing, foam industries, and in electronic applications (electroplating, circuit boards, and metal degreasing) (Almomani et al., 2018; Bailón et al., 2009; Ribeiro et al., 2015).

Physico-chemical and biological waste gas treatment processes (BWGTPs) have been employed for the treatment and removal of VOCs from industrial waste gases (Almomani et al., 2018; Kennes et al., 2009; Rene et al., 2011). The application of any WG treatment process depends on its performance, safety and economic feasibility. Absorption, adsorption, condensation, incineration, and catalytic processes demonstrated high efficiency for the treatment of IWGs (Amoah-Antwi et al., 2020; Cheng et al., 2019; Li et al., 2019; Yang et al., 2019; Zi et al., 2019). However, the regeneration of adsorbents, management and high treatment cost of the produced secondary pollutants and difficult operational conditions limit the large scale applications of these processes (Kennes et al., 2009). Conversely, BWGTPs appear to be more feasible and cost-effective for the treatment of VOCs at concentrations $<$ 5 g/m^3. The BWGTPs can be used to mineralize VOCs at ambient conditions into non toxic products including CO_2 and H_2O (Almomani et al., 2018; Devinny et al., 1998; Kennes and Veiga, 2001, 2013). Biofilter, biotrickling filter, and modified RBC were successfully employed to treat different WGs containing DCM (Bailón et al., 2009; Han et al., 2018; Kennes and Veiga, 2001, 2013; Ravi et al., 2010). Nevertheless, the

* Corresponding author.
E-mail address: falmomani@qu.edu.qa (F. Almomani).

https://doi.org/10.1016/j.jhazmat.2020.123735
Received 11 June 2020; Received in revised form 30 July 2020; Accepted 12 August 2020
Available online 22 August 2020

Nomenclature

$\%DCM_r$	Percentage removal of DCM, %
%RH	Percentage relative humidity, %
C_{OH}	Concentration of hydroxyl radicals, g/m^3
K_i	Adsorption kinetic constant, m^3/g
Q_{max}	Maximum DCM adsorbed on TiO_2, g/m^3
$[DCM]_i$	Inlet DCM concentration, g/m^3
$[DCM]_o$	Outlet DCM concentration, g/m^3
AOPs	Advanced oxidation processes
APHR	Annular photo-reactor
BE	Binding energy, eV
BT	Biological treatment
BWGTPs	Biological waste-gas treatment processes
CB	Conduction bands
CCD-SA	Central composite design-statistical approach
CSTBR	Continuous stirred tank bioreactor
DCM	Dichloromethane
D_p	Average particle diameter, nm
EC	Elimination capacity, $g/m^3 \cdot h$
K_{hv}	Kinetic constant of UV-process
k_{Sch}	Scherrer's constant, 1/s
$PH\text{-}C_L$	Photocatalyst loading, g/m^2
Q_{gas}	Gas flow rate, m^3/h
ROS	Reactive oxygen species
t	Reaction time, min
V	Reactor volume, m^3
VB	Valence bands
VOCs	Volatile organic compounds
WG	Waste gas
α	Reaction order
β	Full-width at half-maximum of the XRD radian
θ	Angel of X-ray radiation, °
λ	Wavelength of the X-ray radiation, nm
τ	Residence time, s

performance and efficiency of standalone BWGTPs may decrease under variable loading patterns, higher concentration of pollutants and sudden/unexpected shock loading conditions. Kennes et al. (2009) and Nabatilan et al. (2010) have shown that sudden fluctuations in WG concentrations and the variation in loading rates pose a challenge for the design and operation of BWGTPs. Additionally, operating the BWGTPs under low contaminant concentration or loading rate demonstrated a decrease in cell activity due to the development of unexpected starvation conditions. Nabatilan et al. (2010) and Hassan and Sorial (2011) recommended adding a non-biological pretreatment step for WGs with varying inlet concentrations. The pretreatment step enhances the overall treatment efficiency, acts as a load equalization stage and reduces the effect of the fluctuations in contaminant concentrations during periodic shock loads.

A review of relevant research work has indicated that adding an activated carbon bed before the BWGTPs minimizes and stabilizes the fluctuations in contaminant concentrations/loads and improves the overall process removal efficiency (Diks and Ottengraf, 1991; Li and Moe, 2005; Nabatilan et al., 2010; Ravi et al., 2010; Weber and Hartmans, 1995). Li and Moe (2005) and Sempere et al. (2010) effectively controlled the dynamic/fluctuating change in the pollutant loads of WGs using a first-stage packed bed tower containing granular activated carbon (GAC) as the adsorbent media. Previously, Moe et al. (2007) showed that adding a GAC bed before BT minimizes the effect of toluene cyclic fluctuations. In this set-up, the GAC bed temporarily adsorbed toluene during high inlet concentration intervals and desorbed it during low concentration periods resulting in an effective load equalization and significant removal efficiency. Despite the high performance, low cost, and simple application of adsorption pretreatment processes, the aforementioned problems associated with the regeneration and disposal of the spent adsorbents and the expensive treatment of secondary pollutants limits its application under such reactor combinations.

The toxicity, low biodegradability, limited solubility in the case of hydrophobic pollutants and high gas-liquid mass transfer resistance of the VOCs are other key operational parameters to consider during the use of the BWGTPs at the field-scale. In these circumstances, destructive processes such as AOPs are highly recommended as a pretreatment option (Amat et al., 2005; Blanco et al., 1999; Nogueira et al., 2005; Sano et al., 2004). Considering this scenario, in addition to acting as a load equalization stage, the AOPs degrade the toxic and recalcitrant contaminants at ambient conditions to simpler products with higher biodegradability and lower toxicity allowing complete treatment in the BWGTPs (Al Momani et al., 2004; Al Momani and Jarrah, 2010; Almomani et al., 2016a). Moussavi and Mohseni (2007) have improved the removal of toluene and *o*-xylene from polluted air using an UV photolysis process as a pretreatment stage to the BT. Koh et al. (2004) confirmed that using a UV process as a pretreatment stage completely degraded the recalcitrant *α*-pinene into water-soluble and more biodegradable intermediates. Mohseni and Zhao (2006) showed that the combination UV-biofilter achieved higher elimination capacities (EC) compared to standalone UV or biofilter processes. Wei et al. (2010) demonstrated that under well-optimized conditions, the UV-TiO_2 process degraded a high concentration of toluene (210 and 500 mg/m^3) into more water-soluble products that can be treated in a BT to achieve 96.7 % removal. Other studies have also shown that, in addition to enhancing the WG removal efficiency, combining AOPs with BT is highly recommended for both practical and economic reasons. Although different photo-catalysts can be used in AOPs, TiO_2 has been used in many versatile applications because of its low costs, easy availability, particle size distribution and good properties (high chemical and thermal stability, non-toxicity, and high photocatalytic activity) (Hisatomi et al., 2014; Yang et al., 2013).

The mechanism of AOPs involves the oxidation of the WGs by the radicals generated from the photonic excitation of the photocatalysts. The TiO_2 absorbs UV irradiations with the energy level $\geq$ 3.2 eV leading to the formation of electron-hole (e^-/h^+) pairs. The electrons move to the surface of the catalyst and react with contaminants, humidity and/or oxygen, generating different radicals [e.g. hydroxyl radicals ($H\dot{O}$)]. The radicals attack the WGs breaking them down into smaller compounds with higher biodegradability and lower toxicity. The total mineralization of the pollutants present in the WG stream to CO_2 and H_2O can be achieved under high oxidation conditions. The degradation efficiency of the AOPs depends on the characteristics of the UV-source, the photocatalyst loading rate ($PH\text{-}C_L$), and the properties of the WGs (composition, flow rate and concentrations) (Almomani et al., 2016b; Pichat, 2003). The United Technologies of Connecticut has established the first of its kind full-scale AOP to treat hydrocarbons stripped from soil or groundwater. The results highlighted the requirements for a larger reactor size to achieve acceptable removal efficiency, which may be prohibitive in some instances.

Given the aforementioned literature overview, a well-established treatment process for the removal of recalcitrant IWGs under different initial concentrations, shock loading rates, and different operational conditions is crucial. Currently, there is a knowledge gap in the literature regarding the effect of key operational parameters on the process performance. Moreover, optimized operational parameters for combined processes (AOPs and BT) require further investigation. Accordingly, this study investigates the use of destruction processes (UV and

UV-TiO_2), BT, and their combination (AOPs-BT) for the treatment of a WG stream contaminated with DCM. As such, the study evaluates the effect of process parameters [gas flow rate (Q_{gas}), inlet DCM concentration ($[DCM]_i$), residence time (τ), photocatalyst loading (PH-C_L) and percentage relative humidity (%RH)] on the process performance. It is noteworthy to mention that, for the first time, a statistically significant central composite design (CCD) approach (CCD-SA) has been used to optimize the process parameters of AOPs-BT. Besides, this study identifies and characterizes the by-products generated from AOPs and correlates them to the treatment mechanism, evaluates the kinetic parameters of AOPs, and presents the overall $\%DCM_r$. The oxidation tests were performed in an annular photo-reactor (APHR), while a continuous stirred tank bioreactor (CSTBR) inoculated with *Hyphomicrobium* spp. was used to carry out the BT tests.

2. Material and methods

2.1. Chemicals

The chemicals used in the preparation of the TiO_2 photocatalyst were tetra-butyl-ortho-titanate [$Ti(OC_4H_9)_4$; Merck, CAS #: 3087−39-6], acetylacetone (C_5H_8O; Merck, CAS #: 123−54-6), and *n*-propanol (C_3H_8O; Merck, CAS #: 71−23-8) purchased from Merck-Qatar. The carbon black powder (diameter ≈ 13 ± 1 nm and surface area ≈ 560 ± 5 m^2/g) was purchased from PlasmaChem (GmbH, Germany).

The chemicals used in the biological reactor's mineral medium were sodium phosphate dibasic dodecahydrate ($Na_2HPO_4{\cdot}12H_2O$; Merck, CAS #: 10039−32-4), monopotassium phosphate (KH_2PO_4; Merck, CAS #: 7778−77-0), magnesium sulfate heptahydrate ($MgSO_4{\cdot}7H_2O$; Merck, CAS #: 10034−99-8), ammonium sulfate [$(NH_4)_2SO_4$; Merck, CAS #: 7783−20-2], calcium chloride ($CaCl_2$; Merck, CAS #: 10043−52-4), manganese sulfate monohydrate ($MnSO_4{\cdot}H_2O$; Merck, CAS #: 10034−96-5), iron(II) sulfate heptahydrate ($FeSO_4{\cdot}7H_2O$; Merck, CAS #: 7782−63-0), zinc sulfate heptahydrate ($ZnSO_4{\cdot}7H_2O$; Merck, CAS #: 7446−20-0), copper(II) sulfate pentahydrate ($CuSO_4{\cdot}5H_2O$; Merck, CAS #: 7758−99-8), boric acid (H_3BO_3; Merck, CAS #:10043−35-3) and sodium molybdate dihydrate ($Na_2MoO_4{\cdot}2H_2O$; Merck, CAS #:1 10102−40-6), purchased from Merck-Qatar.

2.2. Bacterial strains and growth medium

The biological treatment of DCM was performed in a continuous stirred tank bioreactor (CSTBR) using two pure *Hyphomicrobium* strains (re)isolated at UDC (Spain) from another CSTBR (Bailón et al., 2009). These strains exhibited an excellent potential to mineralize DCM under optimal environmental conditions during the preliminary tests. Stock cultures of these strains were grown on Petri dishes and maintained in a chamber with a continuous supply of gas-phase DCM. The CSTBR was operated with a mineral salt medium which was prepared by mixing 4.88 g $Na_2HPO_4.12H_2O$, 1.83 g KH_2PO_4, 0.17 g $MgSO_4.7H_2O$, 0.45 g $(NH_4)_2SO_4$, 0.5 mL of trace minerals, and 1 mL of vitamin solution in 1-L of deionized pure water (18.2 MΩo-cm and 0.055 μS). The pH of the medium was adjusted to 7.0 using 2 N NaOH or concentrated phosphoric acid.

The trace mineral solution was prepared by mixing 5.5 mg $CaCl_2$, 0.15 mg $MnSO_4$. H_2O, 1.5 mg $FeSO_4.7H_2O$, 0.2 mg $ZnSO_4.7H_2O$, 0.2 mg $CuSO_4.5H_2O$, 0.02 mg H_3BO_3 and 3 mg $Na_2MoO_4.2H_2O$ in 1 L distilled water. The vitamin mixture was prepared by dissolving: 0.15 mg folic acid, 0.15 mg biotin, 0.25 mg thiamine, 0.25 mg riboflavin, 0.25 mg nicotinic acid, 0.001 mg vitamin B_{12}, 0.26 mg p-aminobenzoic acid, 0.7 mg pyridoxamine, and 0.25 mg lipoic acid in 1 L of deionized pure water (18.2 MΩo-cm and 0.055 μS). The decrease in the pH of CSTRB due to the formation of HCl during the biological degradation of DCM (Bailón et al., 2009) was neutralized by adding 2 N NaOH.

2.3. Experimental set-up

Fig. 1 displays the experimental set-up used for the treatment of DCM. The set-up consists of two parts: the annular photo-reactor (APHR) and the CSTBR. The APHR was made of a cylindrical tube (ID=5.6 cm and L=55.5 cm) and equipped with a 50 W tubular UV lamp mounted centrally in a glass tube. The effective annular volume for the gas phase reaction was 0.96 L. The UV lamp emitted UV light at a wavelength (λ) of 254 nm. Continuous circulation of cooling water within the APHR jacket was used to control the reactor temperature.

The TiO_2 photocatalyst was coated to the inner side of the APHR following the procedure outlined in our previous study (Almomani et al., 2016a). The procedure can be summarized as follows: 1 g of tetra-butyl-ortho-titanate ($Ti(OC_4H_9)_4$) was mixed with 0.5 mL of acetylacetone (C_5H_8O), 5 mL of n-propanol (C_3H_8O) and 0.5 mL of deionized water at 25 °C and 500 rpm for 60 min. The produced mixture was then mixed with 15 mg of carbon black powder (diameter ≈ 13 ± 1 nm and surface area ≈560 ± 5 m^2/g), at 150 rpm for 30 min, and left standing at a controlled temperature of 25 °C for 2 h to complete the hydrolysis of $Ti(OC_4H_9)_4$ by the chelating agent (C_5H_8O in this study). The generated TiO_2 sol was then used to create a film on the inner side of the APHR using cyclic dipping-withdrawing-heating procedure. At the end of each dipping-withdrawing step, the coated TiO_2 gel film was heat-treated at 500 °C for 1.5 h using an electrical oven. The cyclic film formation was repeated ten times producing a TiO_2 film with different loading rates as determined by the Tencor α-step profiler (Alpha-Step® D-500, USA).

The CSTBR system consists of a 2.5 L jacketed biological reactor (BioFlo 310 autoclavable fermenter, New Brunswick Scientific, Canada) equipped with a gas feeding line that leads to a diffuser to feed the DCM polluted air, a mixer, a line to vent the treated air and a cooling jacket. All the fittings, connections, and tubes were made of either glass or Teflon. The operating volume of the CSTBR was set at 2.0 L allowing 0.5 L as a gas headspace. The Q_{gas} was adjusted in the range of 0.06 to 0.24 m^3/h using a digital flowmeter (ATO-FLOW-MF5700, China) to provide different residence times (τ) within the reactor, namely 0.5, 1, and 2 min, respectively. The biological treatment was carried out at a pH of 7.0, an agitation speed of 400 rpm, a controlled temperature at 30 °C, and a dissolved oxygen (DO) concentration (% saturation) of 80 %.

2.4. Experimental procedure

The treatment of WG containing DCM includes: (1) photolysis using UV-light, (2) photocatalytic oxidation using UV-TiO_2, and (3) combined UV or UV-TiO_2 with BT. The experimental procedure adopted for parts 1 and 2 of this study was conducted as follows: the gas phase stream was produced by bubbling air stream through a vaporization chamber containing pure dichloromethane (DCM). The generated DCM-air mixture was then mixed in a mixing chamber with a pure air stream at differing flow rates to generate a gas phase with DCM concentrations (DCM_i) in the range of 2.0–12.6 g/m^3. Subsequently, the DCM-air stream was passed through the APHR until a steady-state concentration was established. Following this, the UV lamp was switched on and gaseous samples were withdrawn at regular intervals from the inlet and outlet and analyzed for DCM concentrations. Control tests were carried out with TiO_2 alone to determine the amount of DCM absorbed onto the surface of the photocatalyst. The photolysis and photocatalytic oxidation of the DCM-air stream was performed at a controlled temperature by varying the flow rate of cooling water recirculating within the outer jacket of the APHR.

The BT was carried out by feeding the CSTBR with varying inlet concentrations of DCM-air mixture. The startup and acclimatization procedure of the CSTBR has been explained in our previous study (Almomani et al., 2018). For each test, a specific inlet concentration of the DCM-air mixture was bubbled into the reaction medium. The residence times (τ) were controlled in the range 30 s and 120 s by adjusting

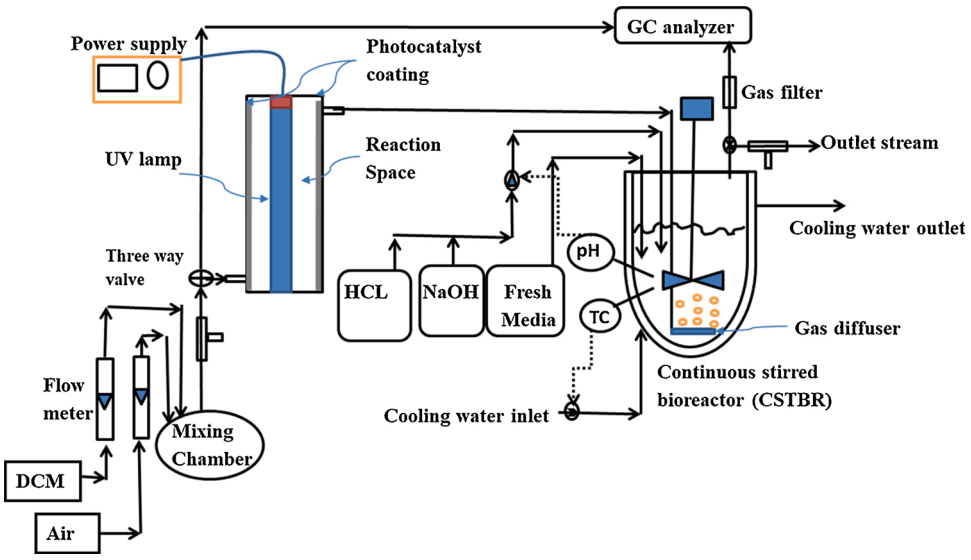

Fig. 1. Schematic experimental set-up of the annular photo-reactor (APHR) and the continuous stirred tank bioreactor (CSTBR).

the flow rate of the inlet gas stream. The pH of the CSTBR was controlled at 7.0 by adding the required amount of 2 N NaOH solution to neutralize the HCl formed during the biological degradation of DCM. The conductivity of the CSTBR medium was maintained at < 20 mS/cm by replacing part of the mineral medium when necessary. The recovered biomass was recycled into the reactor in order to maintain a constant biomass concentration.

The response of the CSTBR to sudden changes in the concentration of DCM was evaluated by performing transient short (2 h)/long (4 h) term shock loads tests. For both tests, the Q_{gas} was maintained at 0.24 m^3/h (τ = 30 s), and the $[DCM]_i$ was < 1 g/m^3 to attain $\%DCM_r$ > 70 %. Subsequently, the $[DCM]_i$ was suddenly increased to 5.5 g/m^3 (inlet loading rate (ILR) ≥ 250 g/m^3·h) for 2 h or 4 h in the short and long term shock loads, respectively, and the $[DCM]_i$, outlet concentration of DCM ($[DCM]_o$), CO_2 evolution, $\%DCM_r$ and EC were determined.

The combined AOPs-BT tests were performed by connecting the outlet gas stream from the APHR to the inlet of the CSTBR. This allowed the gas stream to be treated in the biological process, following the same previously described procedure.

2.5. Central composite design-statistical approach (CCD-SA)

The optimum operating conditions for the oxidation process were determined using CCD-SA, which relies on the central effect of each process parameter on the $\%DCM_r$. Three process parameters including τ, %RH and $[DCM]_i$ were used in the calculations related to the UV process, while an additional fourth parameter (PH-C_L) was added to the calculations related to UV-TiO_2 process. Calculations were based on cubic four-level factorial design ($CFLF^{4k}$) (Eq. 1), which tested the effect of each parameter on $\%DCM_r$. This was based on the central point calculations between the lowest and highest normalized values. The significance of the model was judged using ANOVA (Prism Software V 7.04) to identify the main and interaction effects between the parameters on the $\%DCM_r$.

$$\%DCM_r = A_0 + \sum_{i=1}^{k} b_i X_i + \sum_{i=1}^{k-1}\sum_{j=2}^{k} c_{ij} X_i X_j + \sum_{i=1}^{k} d_{ii} X_i^2 \quad (1)$$

Where X_i, X_j, …., X_k are the input operational parameters ([DCM]i, τ, % RH, PH-C_L), A_0 is the intercept, b_i (i = 1, 2,…, k), c_{ij} (i = 1, 2, …, k-1, j = 1, 2, …, k), and d_{ii} (i = 1, 2, …, k) are the linear, interaction, and squared effect of the process variables on the $\%DCM_r$.

2.6. Analytical methods

The concentrations of DCM were determined using an online GC-FID gas chromatograph (Agilent technology, Model number 7890A, USA) fitted with a 3 mm ID and a 2 m packed column (AT OV101). The injector and detector temperatures were 190 °C and 250 °C, respectively. A humidity analyzer (Omega Engineering) was used to determine the humidity of the gaseous stream. The COD and BOD_5 tests were conducted as per the procedure outlined in the Standard Method (Methods # 5210 and 5220D) (APHA, 1985). A Hach ready-to-use reagent (Product #:2125925) was used in the COD tests, while BOD_5 incubation was carried out in oxy top 300 mL bottles (Thomas Scientific, USA).

The oxidation byproducts after the AOPs were identified using gas chromatography-mass spectrometry (Clarus® SQ 8 GC/MS, PerkinElmer) coupled with built in library. Standard solution of the identified byproducts were used to confirm their presence in the treated effluent. The soluble by-products were collected in a deionized water bath at 10 °C. The by-products were characterized by measuring the chemical oxygen demand (COD), the 5-day biological oxygen demand (BOD_5), and the biodegradability index (Bio_{indx}). The insoluble by-products were determined using GC-FID (Agilent technology, Model number 7890A, USA).

2.7. Characterization of the photocatalysts

Different analytical and characterization techniques including scanning electron microscopy (SEM-EDS, Quanta 600 model, Austria), XRD (Hiltonbrooks, UK), Brunauer-Emmett-Teller (BET, V-Sorb 4800S, USA), XPS (Kratos Axis Ultra, USA) and N_2 adsorption-desorption isotherm were utilized to examine the morphology, surface area, structure and particle size of the TiO_2 photocatalysts.

2.8. Mathematical calculations and performance evaluation

The performance of the AOPS (UV and UV-TiO_2) and the BT in removing DCM were determined by calculating the $\%DCM_r$ (Eq. 2) and the average elimination capacity (EC) (Eq. 3).

$$\%DCM_r = \frac{([DCM]_i - [DCM]_o)}{[DCM]_i} \quad (2)$$

$$EC\left(g/m^3h\right) = t\frac{Q_{gas}\left([DCM]_i - [DCM]_o\right)}{V} \quad (3)$$

Where, $[DCM]_i$ and $[DCM]_o$ are the influent and effluent DCM concentrations (mg/m^3), V is the active volume of the reactor (m^3). Tests were carried in triplicate and the average at 95 % confidence level was used in reporting the results.

The kinetics of UV process was determined using the global reaction kinetics (Eq. 4):

$$-\frac{d[DCM]}{dt} = k_{hv}[DCM]^{\alpha} \quad (4)$$

Where, [DCM] is the DCM concentration at any time, t is the reaction time (min), K_{hv} is the kinetic constant, and α is the order of the reaction. Eq. (3) can be converted to a linear form, as shown in Eq. (5):

$$\ln\left\{-\frac{d[DCM]}{dt}\right\} = \ln\{k_{hv}\} + \alpha\ln[DCM] \quad (5)$$

The reaction kinetics of the UV-TiO_2 process was modeled according to Eq. (6), as proposed by Almomani et al. (2018):

$$-\frac{dC}{dt} = \left\{K_{hv} + \frac{Q_{max}K_i}{1+K_i} + K_{OH}C_{OH}\right\}[DCM] \quad (6)$$

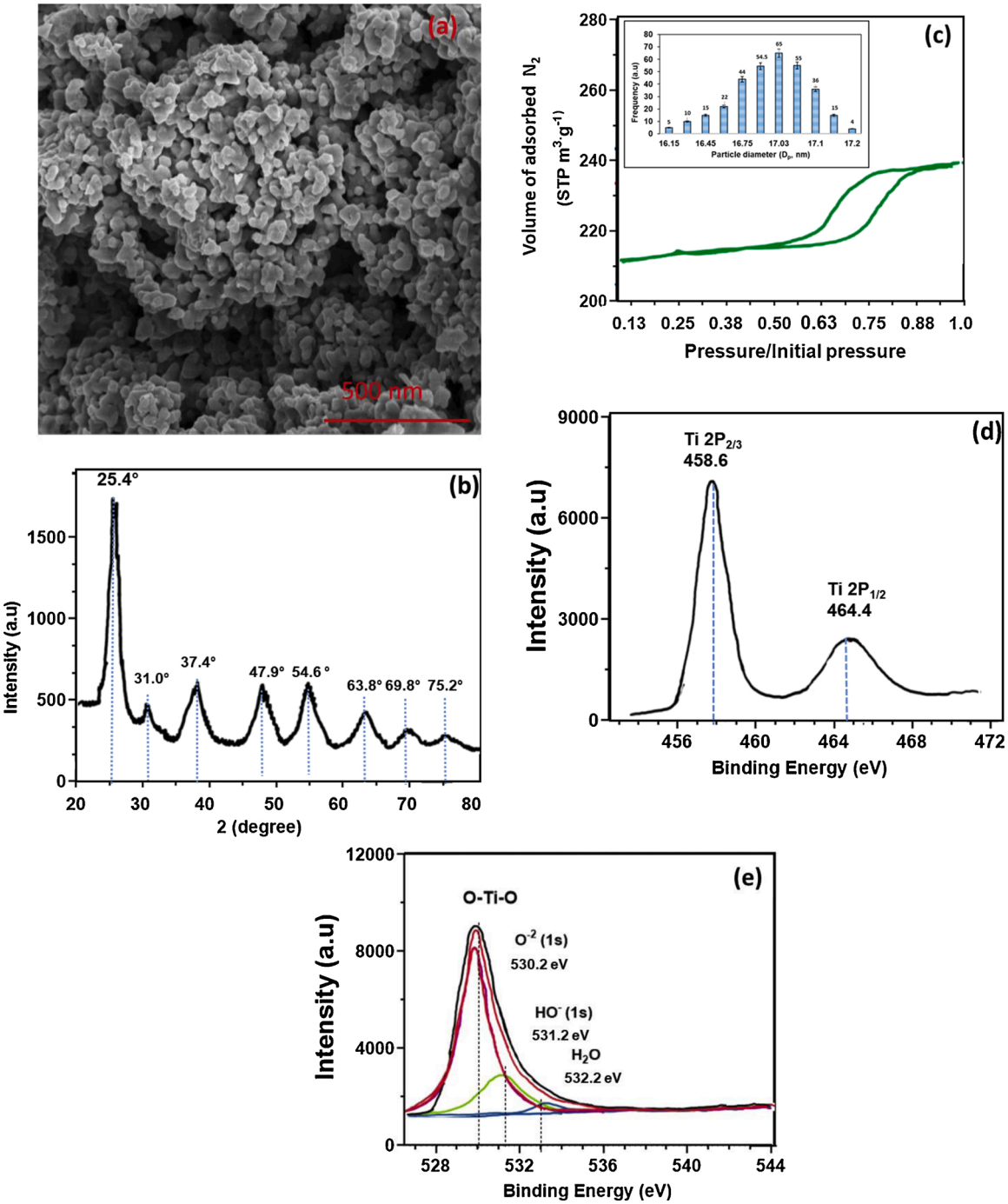

Fig. 2. (a) SEM images of TiO_2 film coated on the inner side of the APHR, (b) XRD patterns of the TiO_2 film, (c) N_2 adsorption-desorption isotherm, inner Figure: particle diameter of the TiO_2 within the film (d) XPS spectrum of the TiO_2 and (e) spectrum of 0 1s in TiO_2.

3. Results and discussion

3.1. Structure and morphology of the TiO_2 film

The SEM images of the TiO_2-film presented in Fig. 2a clearly show the formation of a relatively rough TiO_2 film deposited on the inner side of the APHR. The TiO_2 particles are well-sintered in the film as small crystalline particles with an average particle diameter (D_p) of 17.03 ± 0.06 nm. Since the average D_p of powdered carbon black used in the preparation of the sol was 13 ± 1 nm, it is likely that the particles were aggregated slightly during the calcination process at 500 °C.

The XRD pattern of TiO_2 (Fig. 2b) indicates the presence of peaks at 2θ of 25.4°, 37.8°, 47.9°, 54.6°, 63.8°, 69.8°, 75.2°, corresponding to tetragonal anatase phase, which is the most active phase for photocatalytic application as suggested by Hoffmann et al. (1995). The weak broaden signal at 31.0° corresponds to the rutile phase as compared to the reference diffraction standard card (JCPDS #21−1772). The observed spectrum suggests that TiO_2 underwent a transformation from amorphous to anatase structure during the calcination process, which commonly requires a temperature ≥325 °C. The N_2 adsorption-desorption isotherm measurements presented in Fig. 2c show that TiO_2 exhibited H1-type hysteresis which is the common shape for porous materials. Scherrer's equation (Eq. 7) was used to calculate the crystallite size of TiO_2, which was found to have D_p in the range 16.15–17.20 nm as presented in the inset of Fig. 2c. These values agree with values calculated from SEM measurements. The chemisorption calculations indicated that the specific surface area (A_{sp}) of TiO_2-film was 55.6 m^2/g.

$$D_p = \frac{k_{Sch}\lambda}{\beta cos\theta} \quad (7)$$

where λ is the wavelength of the X-ray radiation ($\lambda = 0.15418$), K is the Scherrer constant ($K = 0.9$), θ the characteristic X-ray radiation ($\theta = 12.7°$) and β is the full-width at half-maximum of the (101) plane (in radians), respectively.

The XPS spectrum of the TiO_2 presented in Fig. 2d shows the energy levels of Ti $2P_{3/2}$ at the binding energy (BE) of 458.6 eV and Ti $2P_{1/2}$ with BE of 464.4 eV corresponding to Ti^{4+} in the TiO_2 structure (Song et al., 2008). The spectrum of O 1s in TiO_2 (Fig. 2f) has three BE peaks at 530.2, 531.2 and 532.1 eV, respectively. The first peak corresponds to O-Ti-O bonds, the second peak was assigned HO^- and the third peak corresponds to physisorbed water molecules on the surface of TiO_2 or oxygen within the O–H groups (Almomani et al., 2020; Trevisan et al., 2014).

3.2. Photolysis and photocatalytic treatment of DCM

The treatment of air polluted with DCM was tested in the UV photolysis and UV-TiO_2 PCO processes. The photolysis test results exhibited a very low $\%DCM_r$ under all the tested concentrations and flow rates. The maximum $\%DCM_r$ did not exceed > 12.5 % for tests carried out at a Q_{gas} of 0.12 m^3/h, τ of 27.6 s and $[DCM]_i \leq 0.45$ g/m^3, and the $\%DCM_r$ decreased to < 4% when the $[DCM]_i$ was increased to > 4.0 g/m^3. The corresponding EC values were in the range of 3–19 $g/m^3{\cdot}h$. The low $\%DCM_r$ achieved by the UV process suggests a low oxidation ability under the tested conditions.

During the photolysis process, however, the UV irradiations reacted with humidity, oxygen, or DCM in the gas phase, generating different radicals that attack DCM leading to its degradation. Previous studies have shown that gaseous reaction media play an important role in the oxidation process. Air, dry or wet, produces different reactive species upon irradiation by UV radiation, inducing different byproducts and removal efficiencies. Koh et al. (2004) showed that during UV-photolysis with dry nitrogen, which is an inert gas and has low UV-light absorption capacity, did not contribute to the formation of radicals nor the photo-degradation process. However, the oxygen present in air absorbs UV at a wavelength ≤ 242 nm, forming different radicals and oxidants, according to reactions (1–3) (Pichat et al., 2000). Adding humidity to the air enhances the production of more hydroxyl radicals following reaction (4), thereby leading to higher $\%DCM_r$. UV-light can also react with DCM producing $\dot{C}H_2Cl$, $\dot{C}l$ and $\dot{C}H_2^{\cdot}$ as per the reactions (5) and (6) and contribute to the total DCM degradation.

$$O_2 + h\nu \xrightarrow{\lambda \leq 242\ nm} \langle O\ (^1D)\ O\ (^1P)\ \rangle \text{ (Reaction 1)}$$

$$\langle O\ (^1D)\ O_2\rangle + M \xrightarrow{\lambda \leq 242\ nm} \langle O_3M\rangle\ M : N_2\ or\ O_2 \text{ (Reaction 2)}$$

$$\langle O\ (^1D)\ O\ (^1D)\ \rangle + M \xrightarrow{\lambda \leq 242\ nm} \langle O_2M\rangle \text{ (Reaction 3)}$$

$$H_2O + h\nu \xrightarrow{\lambda \leq 242\ nm} \rightarrow H^{\cdot} + OH^{\cdot} \text{ (Reaction 4)}$$

$$CH_2Cl_2 \xrightarrow{h\nu} \dot{C}H_2Cl + \dot{C}l \text{ (Reaction 5)}$$

$$\dot{C}H_2Cl \xrightarrow{h\nu} \dot{C}H_2^{\cdot} + \dot{C}l \text{ (Reaction 6)}$$

The low $\%DCM_r$ observed by the photolysis process suggests low reactivity between UV and the gas stream in the APHR leading to low production of radicals to achieve significant $\%DCM_r$. In addition, reactions (1) to (6) indicate that photo-oxidation played a predominant role in the DCM degradation process, which was more important than the direct photolysis process. To verify this trend, additional tests were carried out using $[DCM]_i < 0.23$ g/m^3, and the observed $\%DCM_r$ increased to 22.5 % ($Q_{gas} = 0.12$ m^3/h and $\tau = 27.6$ s). Almomani et al. (2018) studied the treatment of DCM in photolysis processes using two UV light sources emitting irradiation at wavelengths (λ) of 254 and 350 nm. The $\%DCM_r$ reported for tests conducted with a light source of λ = 254 nm was ~37.8 % and no more than 6.7 % was achieved for tests carried out with a light source of λ = 350 nm. The study concluded that the acceptable $\%DCM_r$ for trials with UV at λ = 254 nm was due to the ability of DCM-air mixture to directly absorb UV at this wavelength, generating different radicals (reactions 1 and 6) to breakdown the DCM into smaller byproducts. It should be highlighted that the low $\%DCM_r$ reported in this study in comparison with the results achieved by Almomani et al. (2018) is due to the operation of APHR at higher $[DCM]_i$, Q_{gas}, and shorter τ. While the DCM photolysis carried out in the present study was performed at a $[DCM]_i$ of 0.45 g/m^3, Q_{gas} of 0.12 m^3/h and τ of 27.6 s, while the previous work was tested at 0.100 g/m^3, 0.072 m^3/h and 60 s, respectively.

The UV-TiO_2 process demonstrated a substantial enhancement in the oxidation of DCM. The reported $\%DCM_r$ ranged from 15 ± 0.5 to 71 ± 1.5 % due to the contribution of TiO_2 to the production of more radicals, which led to the degradation of DCM. Tests carried out with $[DCM]_i \leq 0.45$ g/m^3, Q_{gas} of 0.12 m^3/h and τ of 27.6 s exhibited a $\%DCM_r$ as high as 70 %, and it decreased to the range of 27%–44% for the tests carried out with $[DCM]_i \geq 4.2$ g/m^3.

The photocatalytic oxidation of DCM starts with the photoexcitation reaction. In this reaction, the TiO_2 absorbs UV photons with an energy ≥ 3.2 eV, leading to the transfer of electrons from the valence bands (VB) to the conduction bands (CB) generating electron-hole (e^-/h^+) pairs (reaction 7). The photo-generated electrons and holes can take several pathways including the recombination on the surface or bulk of the TiO_2; electron acceptors might be reduced by the electrons and electron donors could be oxidized by the holes. The reactions between the photo-generated electron-hole and O_2 and/or H_2O can produce different reactive oxygen species (ROS) such as $HO^{\cdot}$, $O_2^{\cdot -}$ and $HOO^{\cdot}$ (reactions 8–10). The $HOO^{\cdot}$ in reaction (10) acts as an electron acceptor and increases the chance for the production of hydrogen peroxide (H_2O_2). The generated H_2O_2 contributes to the formation of more hydroxyl radicals and reduces the recombination rate of electrons and holes by capturing photo-induced electrons, thus improving the degradation of DCM (reactions 12–14). The oxidation (8) and reduction reactions (9) that occur on the surface of the photo-excited TiO_2 also contributes to the degradation of DCM. Therefore, it can be seen that, photo-excitation of TiO_2 by UV leads to the formation of hydroxyl radicals by oxidizing the adsorbed water or adsorbed −OH to degrade the DCM (Han et al., 2013; Tseng et al., 2010). The UV-TiO_2 photocatalytic oxidation of DCM

includes several processes such as the formation and recombination of electrons and holes, the adsorption of DCM, chemical oxidation/degradation, and the desorption of the formed byproducts (Feng et al., 2010). Although the $[DCM]_i$ used in this study is two orders of magnitude higher than the concentration used in a previous work (Almomani et al., 2018), the achieved $\%DCM_r$ was comparable at ~ 64.6 %.

(Photo-excitation) $TiO_2 \xrightarrow{h\nu \leq 390nm} e^-_{CB} + h^+_{VB}$ (Reaction 7)

(Oxidation reaction) $OH^- + h^+_{VB} \rightarrow HO^{\bullet}$ (Reaction 8)

(Reduction reaction) $(O_2)_{ads} + e^-_{CB} \rightarrow O_2^{\bullet -}$ (Reaction 9)

(Protonation of superoxide) $O_2^{\cdot -} + H^+ \rightarrow HOO^{\cdot}$ (Reaction 10)

(Electron scavenger) $HOO^{\cdot} + e^-_{CB} \rightarrow HOO^-$ (Reaction 11)

(Formation of H_2O_2) $2h^+_{VB} + 2\,H_2O \rightarrow 2\,H^+ + H_2O_2$ (Reaction 12)

(Formation of $OH^{\cdot}$ radical) $H_2O_2 \rightarrow 2\,OH^{\cdot}$ (Reaction 13)

(Water photolysis & radical formation from) $H_2O \xrightarrow{h\nu} \dot{H} + \dot{O}H$ (Reaction 14)

(DCM oxidation) $CH_2Cl_2 + \dot{O}H \rightarrow H_2O + CHCl_2$ (Reaction 15)

Fig. 3 presents the effect of various parameters, including $[DCM]_i$, τ, Q_{gas}, %RH, and PH-C_L on the $\%DCM_r$ during the treatment of DCM by the UV and UV-TiO_2 processes. As the Q_{gas} entering the APHR is related to the τ, these two parameters were studied in the same set of experiments. Fig. 3a presents the $\%DCM_r$ achieved by these processes as a function of τ and at different $[DCM]_i$. The %RH and PH-C_L TiO_2 during this set of experiments were 35 % and 5 g/m^2, respectively. Increasing the τ has a small effect on the performance of the UV process for tests conducted with $[DCM]_i$. ≤ 0.45 g/m^3 and there was a negligible effect at higher concentrations. Under all the tested values of τ, the $\%DCM_r$ was < 12.5 %, except for the tests carried out at $[DCM]_i \leq 0.2$ g/m^3, where up to 22.5 of $\%DCM_r$ was reported. For the UV-TiO_2 process, it was observed that the $\%DCM_r$ increased by ~ 1.5-fold as the τ increased from 6.9 ($\%DCM_r$ ~ 53.4 ± 0.5) to 55.2 s ($\%DCM_r$ ~ 79.9.4 ± 2.5). The observed trends are due to an increase in the time the DCM stays in the APHR to react with the generated radicals and achieve higher removal efficiency. Conversely, the low $\%DCM_r$ observed at lower τ could be

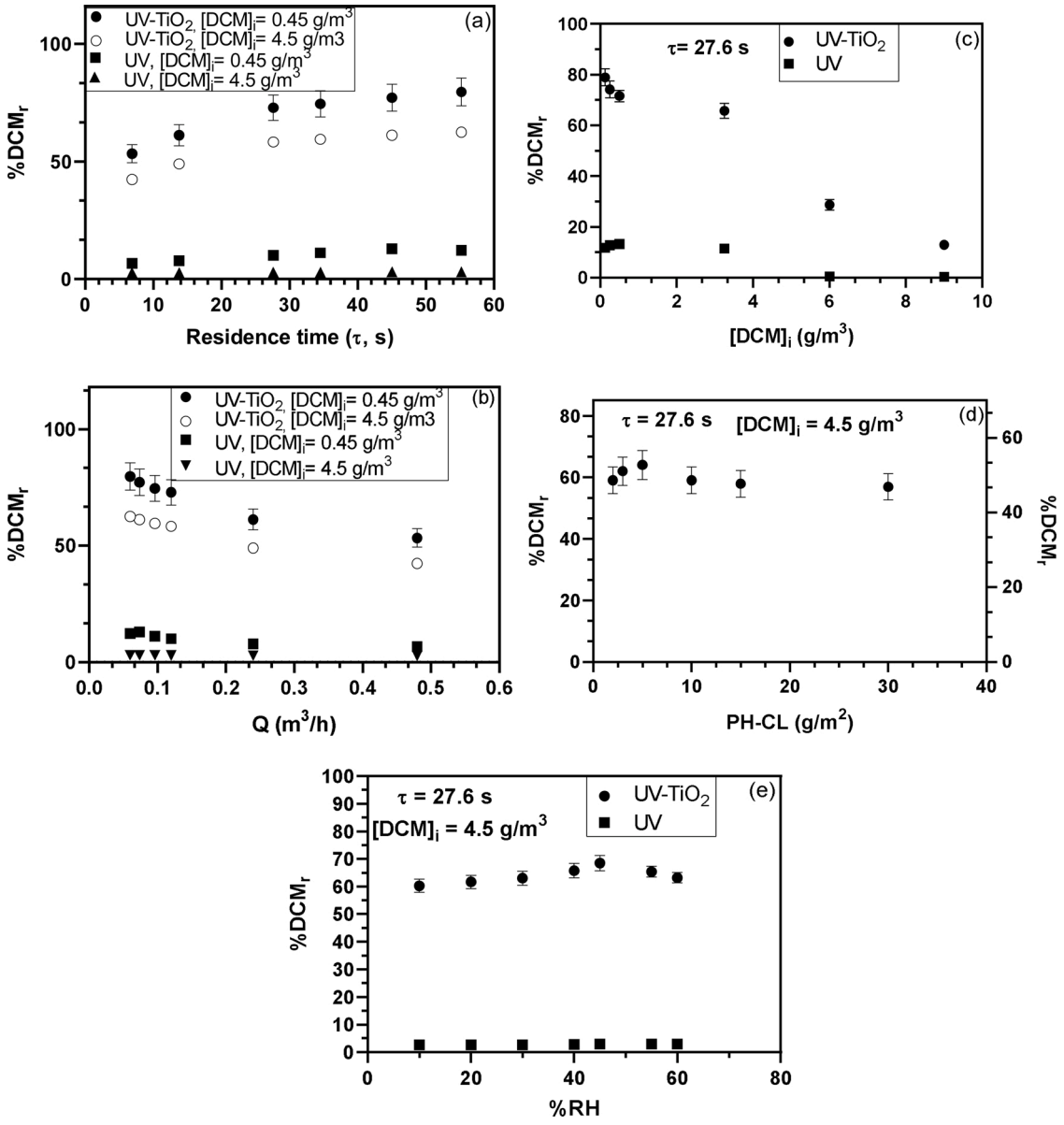

Fig. 3. Effect of process variables on the $\%DCM_r$ in the UV and UV-TiO_2 processes, (a) residence time (τ), (b) gas flow rate (Q_{gas}), (c) initial concentration of DCM, (d) photocatalyst loading (PH-C_L), and (e) percentage relative humidity (%RH).

attributed to the low contact time between DCM and the generated radicals.

Fig. 3b shows that, increasing the Q_{gas} of the UV process from 0.06 m^3/h to 0.24 m^3/h resulted in a 5% and 1.5 % decrease in the reported % DCM_r for tests conducted at a $[DCM]_i$ of 0.45 g/m^3 and 4.5 g/m^3, respectively, suggesting a negligible effect of Q_{gas} on the performance of this process. Although higher $\%DCM_r$ was expected for tests carried out at low Q_{gas}, the low oxidation efficiency of the UV process might mask/hinder this effect. The UV-TiO_2 process exhibited different trends (Fig. 3b), i.e. increasing the Q_{gas} from 0.06 to 0.1 m^3/h led to a sharp decrease in the reported $\%DCM_r$. Thereafter, the gas flow rate had a lesser effect on the observed $\%DCM_r$. Increasing the gas flow rate from 0.06 m^3/h to 0.24 m^3/h caused a 15 % and 20.2 % decrease in the % DCM_r for tests carried out at a $[DCM]_i$ of 0.45 g/m^3 and 4.5 g/m^3, respectively. The obtained results suggest that Q_{gas} is an important factor that affected the degradation of DCM into other byproducts and soluble intermediates (Sánchez et al., 1999). In addition, the results indicated that high removal/degradation of DCM can be achieved for $Q_{gas} \leq 0.10$ m^3/h.

The effect of the $[DCM]_i$ on the $\%DCM_r$ of the UV and UV-TiO_2 processes is presented in Fig. 2c. Increasing the $[DCM]_i$ from 0.125 g/m^3 (low) to 9 g/m^3 (high) decreased the $\%DCM_r$ of the UV and the UV-TiO_2 processes, wherein a significant effect was observed for the UV process. As the degradation of DCM depends on the presence of ROS, the significant decrease in $\%DCM_r$ when increasing the $[DCM]_i$ in the UV process is attributable to the limited generation of radicals to react with the high concentration of DCM and achieve satisfactory degradation. In the case of the UV-TiO_2 process, the photo-excitation reaction reacts with DCM stream in the presence of humidity that contributes to the formation of different ROS leading to a series of reactions that contribute to DCM degradation and achieve high $\%DCM_r$. Thus, as the $[DCM]_i$ increases, a higher concentration of radicals is required to achieve reasonable removal of DCM in the gas phase.

Fig. 3d shows that increasing the PH-C_L from 2 g/m^2 to 5 g/m^2 exhibited a slight improvement (~9.6 %) in the reported $\%DCM_r$. However, tests carried out with a PH-$C_L \geq 10$ g/m^2 showed no significant improvement in the $\%DCM_r$. Despite a 3-fold increase in the catalyst load, from 10 g/m^2 to 30 g/m^2, the reported $\%DCM_r$ was in the same order of magnitude (63 ± 2%). The effect of %RH on the $\%DCM_r$ by UV and UV-TiO_2 is presented in Fig. 2e. Due to the low oxidation potential of the UV process, the effect of the %RH cannot be recognized. Under all the tested %RH, the $\%DCM_{r(s)}$ achieved by the UV-process were in the same order of magnitude. The UV-TiO_2 process exhibited a notable increase in the $\%DCM_{r(s)}$ by increasing the %RH of the gas stream up to 45 %, while a slight decrease was observed for tests performed at $\%RH \geq 50$ %. As discussed above, the photo-excitation reaction and the generated electron-hole (e^-/h^+) pairs enable the TiO_2 photocatalyst to react with either O_2 and/or water vapor to produce radicals (OH $^{\bullet}$and $\bullet O_2^-$) following reactions (7) to (13), leading to higher $\%DCM_r$ (Al Momani and Jarrah, 2009; Al Momani, 2007b). However, excessive %RH can cause competitive adsorption between water and DCM on the active sites of the TiO_2 and thus reduce the photocatalytic oxidation efficiency and decrease the reported $\%DCM_r$. Similar trends were observed by Obee and Hay (1997) and Al Momani and Jarrah (2009).

The effect of different process variables on the $\%DCM_r$ was analyzed using ANOVA (*F*-Fischer's variance ratio, *P*-Probability value). The results revealed that τ, $[DCM]_i$, %RH and PH-C_L are the major factors affecting the UV-TiO_2 performance in terms of $\%DCM_r$ with statistical preferences ordered as τ (*F*: 5363, $P < 0.005$) > $[DCM]_i$ (*F*: 1834, $P < 0.005$) > %RH (*F*: 1632, $P < 0.005$) > PH-C_L (*F*: 353, $P < 0.005$).

Another set of experiment was performed to identify the best conditions to achieve a steady-state $\%DCM_r$ by the UV and UV-TiO_2 processes. A CCD-SA was employed to determine the significant terms that needed to be fit into the cubic four-level factorial ($CFLF^{4k}$) model of % DCM_r. Experimental results were incorporated within Eq. (8) and only terms with *P* values < 0.1 were accepted to be statistically significant. In addition, the root mean square (RMS), and the difference between the calculated and the predicted $\%DCM_r$ were used to determine the significance of the process parameters. Table 1 presents the results of the ANOVA results of the $CFLF^{4k}$ model of $\%DCM_r$. The results revealed that AOPs depends on the τ (denoted as x_1), PH-C_L (denoted as x_2), $[DCM]_i$ (denoted as x_3) and %RH (denoted as x_4) to achieve a steady-state % DCM_r. The ANOVA analysis for both the UV-TiO_2 system indicated *P* values < 0.1, RMS $\leq 0.22 \times 10^{-4}$, a Prob > *F* value lower than 0.065 and a lack of fit at 1.6×10^{-5}. Comparable values of $P < 0.1$, RMS $\leq 0.169 \times 10^{-4}$, a Prob > *F* (< 0.066) and lack of fit at 1.1×10^{-5} were observed for the UV process.

$$\%DCM_r = A_0 + b_1x_1 + b_2x_2 + b_3x_3 + b_4x_4 + c_{1,2}x_1x_2 + c_{1,3}x_1x_3 + c_{2,3}x_2x_3 + d_1x_1^2 + d_2x_2^2 + d_3x_3^2 + d_4x_4^2 \quad (8)$$

The calculated parameters and the experimental results under the optimized conditions were treated mathematically and the results indicated that the steady-state effluent concentration of DCM can be achieved after 5 min of operation of the APHR. Such a short time in achieving steady-state removal of DCM is advantageous when pollutant loads fluctuate in the WG. Moreover, a steady-state effluent concentration is required when the APHR is connected to the CSTBR. It was observed that DCM was degraded up to a maximum of 70 % and mineralized up to ~ 27 %–35 %, which suggests the degradation of DCM to easily degradable intermediates. Previous research has recommended the use of a stronger oxidation process to achieve complete mineralization of recalcitrant VOCs in the gas phase (Chen et al., 2010; Cheng et al., 2011; Yang et al., 2007). However, most of the previous works showed that the complete mineralization of some pollutants by AOPs will not be economically feasible. Instead, these processes can be employed to reduce the toxicity and increase the biodegradability of the WG streams that can later be treated with a simple and cheap biological process (Al Momani, 2007a; Contreras et al., 2003; Farhanian et al., 2013; Muñoz-Batista et al., 2013; Zhang et al., 2014).

The low mineralization capacity of the UV-TiO_2 process may be due to the formation of a hydroxyl radical scavenger, such as chlorine, which could reduce the DCM mineralization. Moreover, the generated oxidation by-products can compete with the targeted compound for photons, which reduces the DCM mineralization. The accumulation of intermediates as a function of DCM conversion can increase this effect over time. Additionally, the intermediates of the oxidation process might absorb the incident light, which can lead to a decrease in DCM removal and mineralization. However, total mineralization is not required by AOPs as long as the produced oxidation byproducts have less toxicity and higher biodegradability than the original DCM.

The kinetic parameters of the UV process were determined according to the formula shown in Eq. (5). The value of α was approximately one and the estimated *k* values were in the range of 0.5 ± 0.35–3.3 ± 0.35 1/min. The values of *k* suggest that the kinetics of the UV process depends on the initial concentration of DCM. The kinetic constants for DCM in the UV process are higher than the values reported for other VOCs. Feiyan et al. (2002) showed that the kinetics of the UV process during the treatment of chlorinated organics [carbon tetrachloride (CTC) and trichloroethylene (TCE)] in the gas phase follows first-order kinetics with a rate constant in the range of 0.09 to 0.12 1/min and 0.06 to 0.27 1/min for CTC and TCE, respectively. However, the obtained results are not consistent with the results found by Lau et al. (2007), wherein the authors reported two-stage pseudo-first-order kinetics during the degradation of pesticides by the UV process.

The kinetics of the UV-TiO_2 process were determined according to Eq. (6). The amount of DCM adsorbed on the TiO_2 was measured in a separate experiment and it did not exceed 2% under all the tested laboratory conditions. Thus, Eq. (6) was reduced to Eq. (9), as follows:

$$-\frac{dC}{dt} = [K_{h\nu} + K_{OH}C_{OH}]C \quad (9)$$

Table 1
ANOVA results of the cubic four-level factorial design.

Term	Coefficient	UV-TiO_2 RMS $\times 10^4$	*P*-value	Prob > *F*	Coefficient	UV RMS $\times 10^4$	*P*-value	Prob > *F*
b_1	5.66	0.11	<0.1	0.041	5.00	0.085	<0.1	0.041
b_2	1.29	0.15	<0.1	0.033	0.28	0.116	<0.1	0.033
b_3	8.33	0.22	<0.1	0.065	9.73	0.169	<0.1	0.066
b_4	4.32	0.10	<0.1	0.023				
$c_{1,2}$	−0.05	0.12	<0.1	0.043	−0.04	0.092	<0.1	0.043
$c_{1,3}$	−0.40	0.09	<0.1	0.055	−0.50	0.069	<0.1	0.056
$C_{2,3}$	0.15	0.05	<0.1	0.031	0.16	0.039	<0.1	0.031
d_1	−1.60	0.13	<0.1	0.023	−1.19	0.100	<0.1	0.023
d_2	−0.007	0.20	<0.1	0.054	−0.0001	0.154	<0.1	0.055
d_3	−7.93	0.06	<0.1	0.046	−7.90	0.046	<0.1	0.046
d_4	−0.63	0.09	<0.1	0.033				
A_0	53.65	0.22	<0.1	0.024	2.65	0.169	<0.1	0.024
Residual	0.0006		<0.1		0.0002		<0.1	
Lack of Fit	1.6×10^{-5}		<0.1		1.1×10^{-5}		<0.1	

As the ROSs (e.g. hydroxyl radicals) are self-generated within the reaction and depends on %RH, Eq. (9) can be converted into Eq. (10), as follows:

$$\ln\left\{-\frac{dC}{dt}\right\} = \ln\{K_{h\nu}\} + \ln(RH)C \tag{10}$$

The evolution of [DCM] as a function of time exhibited compatibility with Eq. (10), which suggests that the proposed kinetic model is acceptable. Table 2 includes the kinetic rate constants of the UV and UV-TiO_2 process during the oxidation of DCM. The results showed that the rate constants of UV-TiO_2 ranged from 1.34 ± 0.35–23.34 ± 0.35 L/mole, which is 1.2–9.1-fold higher than the UV process (0.5 ± 0.35–3.3 ± 0.35 min^{-1}). The kinetic rate data confirms the high oxidation potential of the UV-TiO_2 in the degradation of the DCM compared to the UV process. The kinetic rate constants of the UV-TiO_2 are higher than the values reported by Almomani et al. (2018) during the solar oxidation of DCM. The high reaction rate can be related to the high photo-excitation rate of TiO_2 by UV irradiation when compared to visible light. The photo-excitation reaction of TiO_2 begins by absorbing photons with energy greater or equal to its bandgap energy (≈3.2 eV) to transfer electrons from the VB to the CB leading to the production of electronic vacancies (EVs) and holes. The transferred electrons and the produced holes react with water and oxygen to initiate the degradation of DCM. As the solar absorption capacity of TiO_2 under solar irradiation light is low, the production of ROSs will also be correspondingly low. Therefore, the DCM oxidation under solar irradiation was not significant. The kinetic data also suggest that the oxidation of DCM via the UV-TiO_2 process occurs through two mechanisms: (i) oxidation processes carried out at low %RH begins with the transfer of electrons from the surface of TiO_2 to DCM and (ii) O_2 generating different radicals (e.g. $\dot{C}H_2Cl$, $\dot{C}l$, $\dot{C}H_2^{\cdot}$ and $O_2^{\cdot -}$) that react with DCM leading to its degradation. Therefore, for processes operated under low %RH, the concentration of DCM plays an important role in the production of radicals and enhancing DCM removal. From a process design perspective, this can be achieved using a tubular reactor with a side stream. On the other hand, oxidation processes operating at high %RH will have an additional reaction between the photo-excited TiO_2 and water vapor producing more radicals that leads to significant $\%DCM_r$.

3.3. Proposed mechanism for the oxidation of DCM

Fig. 4a presents the proposed mechanism of DCM oxidation based on the identified intermediates and final products. The photo-excitation reaction by UV or UV-TiO_2 systems attack the DCM containing air mixture generating different organic radical species (Fig. 4b), including, $HO^{\cdot}$, $O_2^{\cdot -}$, $HOO^{\cdot}$ $\dot{C}l$, $\dot{C}H_2$, and $\dot{C}H_2Cl$. During some stages, $\dot{C}l$ can react with $\dot{H}$ to form HCl, which was noticed by a decrease in the pH of the quenching water and detected within the final products as H^+ and Cl^-. The $\dot{C}H_2$ reacts with the water producing $\dot{O}H$, which subsequently reacts with DCM producing acetic acid (CH_3COOH), formic acid (HCOOH) and hydroxyl acid; thereafter, this dissociates to produce CO_2 and H_2O. The reaction between $\dot{O}H$ and DCM can also produce small organic compounds such as aldehyde (HCOH) and form acetic acid (CH_3COOH). Radicals such as $\dot{C}H_3$ originated from $\dot{C}H_2$ react with $C\dot{O}OH$ producing CO_2 and H_2O. Moreover, radicals such as $O_2^{\cdot -}$, $\dot{O}H$ and $HOO^{\cdot}$ produced from water photolysis or photo-excitation reactions can also react with DCM producing glyoxylic acid (CHOCOOH), acetic acid, and HCl, respectively.

The products generated from the degradation of DCM were passed through a water bath and the effluent gases were tested using a GC. The results revealed that most of the DCM oxidation products were soluble in water. The GC measurements showed limited organic matters (OMs), i.e. ≤ 0.5 mg/L, in the gas streams after the water bath. The obtained results support the feasibility of using UV or UV-TiO_2 as an upstream or first-stage process to convert DCM into more soluble, less toxic and highly biodegradable products that could be treated in a subsequent biological process to improve the overall $\%DCM_r$. To guarantee effective BT, the level of biodegradability and the concentration of these products should be examined on a case-to-case basis because a typical WG usually contains a mixture of pollutants. The products collected in the water bath were characterized based on the COD, BOD_5, and their biodegradability index (Bio_{indx}), as shown in Table 2. The values presented in Table 2 show that the concentrations of organic matters, represented as COD and BOD_5, increased as the degradation of DCM increased, confirming the capture of these products in the water bath. The COD of the water bath for the tests conducted with UV ranged from 5.7 mg O_2/L to 30.1 mg O_2/L and the BOD_5 ranged from 4.2 mg O_2/L to 24.8 mg O_2/L, respectively. The Bio_{indx} increased linearly with an increase in the $\%DCM_r$. Tests carried out with the UV process showed Bio_{indx} in the range 0.18 to 0.89, which was considered high compared to 0.15 for pure DCM. The UV-TiO_2 process exhibited (approximately) a 3-fold increase in COD (26–486 mg/L) and BOD_5 (19–351 mg/L) concentrations and a significant enhancement in the Bio_{indx} (0.20 to 0.93). The noticeable improvement in the Bio_{indx} after the UV-TiO_2 process was mainly due to the high oxidation efficiency that degraded DCM into more soluble and biodegradable products, which can be treated by conventional gas-washing methods and fed through subsequent biological processes to achieve complete removal of pollutants in the IWG.

Table 2
Summary of DCM oxidation, kinetic data, and characterization of by-products and the performance of combined oxidation-biological processes.

$[DCM]_i$ (g/m^3)	τ (sec)	Q_{gas} (m^3/h)	$\%DCM_r$ (%)	ILR ($g/m^3.h$)	C_{out} (g/m^3)	EC_{oxid} ($g/m^3.h$)	% RH	COD (mg/L)	BOD_5 (mg/L)	Bio_{indx}	K (min)	RE_{Bio} (%)	RE_{Bio} (%)	$C_{out,bio}$	EC_{bio} ($g.m^{-3}\ h^{-1}$)	$\%CDM_{r,otal}$ (%)
	UV											CSTBR				
0.25	30.1	0.11	11.30 ± 0.2	13.75	0.22	3.2		5.7	4.2	0.57	0.57	87 ± 2	62.2	0.08	7.58	66.43
0.25	60.2	0.06	19.3 ± 0.2	6.88	0.20	2.8		9.7	7.3	0.97	0.97	91 ± 2	96.5	0.01	5.35	97.18
0.25	120.0	0.03	31.1 ± 0.1	3.45	0.17	2.3		15.9	14.0	0.88	1.59	96 ± 2	97.1	0.00	2.29	98.02
0.45	30.1	0.11	13.50 ± 0.2	24.75	0.39	6.9		12.1	9.0	0.67	1.21	88 ± 2	73.7	0.10	15.79	77.21
0.45	60.2	0.06	19.2 ± 0.2	12.38	0.36	5.1		17.6	15.5	0.88	1.76	93 ± 2	98.2	0.01	9.77	98.55
0.45	120.0	0.03	31.3 ± 0.1	6.21	0.31	4.1		28.2	25.1	0.89	2.82	96 ± 2	97.3	0.01	4.15	98.15
4.6	30.1	0.11	2.0 ± 0.6	253.00	4.50	11.8		20.6	15.4	0.11	2.06	88 ± 2	12.3	3.94	30.39	14.25
4.6	60.2	0.06	2.0 ± 0.6	126.50	4.47	7.4		25.8	19.3	0.14	2.58	93 ± 2	15.4	3.78	18.94	17.77
4.6	120.0	0.03	3 ± 0.11	63.48	4.46	4.0		27.6	20.7	0.15	2.76	96 ± 2	16.5	3.73	10.16	19.01
0.25	30.1	0.11	12.7 ± 0.2	13.75	0.22	3.6		6.3	4.7	0.63	0.63	96 ± 2	69.6	0.07	8.36	73.43
0.45	30.1	0.11	14.5 ± 0.1	24.75	0.38	7.5		13.1	9.8	0.73	1.31	93 ± 2	79.8	0.08	16.88	82.69
4.6	30.1	0.11	3.6 ± 0.1	253.00	4.43	19.0		33.1	24.8	0.18	3.31	96 ± 2	19.8	3.56	48.29	22.68
	$UV\text{-}TiO_2$											CSTBR				
0.25	30.1	0.11	52.50 ± 0.2	13.75	0.118	15.1		26.4	19.8	0.79	1.32	87 ± 2	94.9	0.006	6.2	97.6
0.25	60.2	0.06	73.3 ± 0.2	6.875	0.066	10.6	35	36.9	0.9	0.93	1.84	96.7	99.6	0.001	1.8	99.9
0.25	120.0	0.03	77.3 ± 0.2	3.45	0.055	5.6		38.9	36.2	0.93	1.95	97.5	95.2	0.003	0.7	98.9
0.45	30.1	0.11	53.50 ± 0.2	24.75	0.210	27.5	35	48.0	36.0	0.80	2.40	98 ± 2	99.2	0.002	11.5	99.6
0.45	60.2	0.06	73.2 ± 0.2	12.375	0.117	19.1		66.7	61.3	0.92	3.33	93 ± 2	96.3	0.004	3.1	99.0
0.45	120.0	0.03	77.0 ± 0.1	6.21	0.101	10.0		69.8	64.9	0.93	3.49	96 ± 2	98.7	0.001	1.4	99.7
4.6	30.1	0.11	36.0 ± 0.6	253	2.922	192.3		335.6	251.7	0.55	16.78	88 ± 2	94.7	0.155	152.2	96.6
4.6	60.2	0.06	50.0 ± 0.6	126.5	2.257	134.2		468.6	351.5	0.76	23.43	93 ± 2	96.8	0.073	60.1	98.4
4.6	120.0	0.03	42.9 ± 0.11	63.48	2.667	55.6		386.7	290.0	0.63	19.33	96 ± 2	98.6	0.037	36.3	99.2
0.25	30.1	0.11	53.7 ± 0.2	13.75	0.116	15.4		26.8	20.1	0.81	1.34	96 ± 2	99.5	0.001	6.3	99.8
0.45	30.1	0.11	54.2 ± 0.1	24.75	0.206	28.0		48.8	36.6	0.81	2.44	93 ± 2	99.3	0.001	11.2	99.7
4.6	30.1	0.11	37.1 ± 0.1	253	2.892	195.7		341.5	256.1	0.56	17.08	96 ± 2	95.6	0.127	152.1	97.2
9	60.0	0.06	13.7 ± 0.1	248.4	7.780	70.1		243.9	183.0	0.20	12.20	96 ± 2	96.4	0.280	207.0	96.9

3.4. Biological treatment of DCM

The BT of DCM was investigated in four distinct stages as outlined in Table 3. The combined effects of $[DCM]_i$ and Q_{gas} as key performance parameters during each phase are presented in Fig. 5a. During phase I, i.e. the acclimation phase, the CSTBR was operated with a low initial concentration of DCM (0.27–4 g/m^3) and Q_{gas} of 0.12 m^3/h ($\tau = 60$ s) to allow the system to achieve a steady-state removal of DCM. The increase in the $[DCM]_i$ and inlet loading rate (ILR) was correlated to the minimum acceptable $\%DCM_r \geq 65$. Considering this condition, the $[DCM]_i$ and the inlet loading rate (ILR) were increased, during the initial 8 days of operation, from 0.27 to 2.0 g/m^3 and 16.3–120.1 $g/m^3.h$, respectively, achieving $\%DCM_r$ and EC in the range of 24.5 %–91.4 %, and 16.3–120.1 $g/m^3.h$, respectively. The $[DCM]_i$ and ILR were then increased on day 9 to 2 g/m^3 and 140 $g/m^3.h$ achieving a $\%DCM_r$ and EC of 92.5 % and 130 $g/m^3.h$., respectively. From days 10–28, the $[DCM]_i$ and ILR were increased gradually from 2.01 to 4.0 $g/m^3.h$ and 180.3 to 240.3 $g/m^3.h$, achieving a maximum $\%DCM_r$ and EC of 97.6 % and 234.0 $g/m^3.h$, respectively. The obtained results indicate that the *Hyphomicrobium spp.* were able to utilize DCM as a carbon source and achieve very high removal efficiencies for $[DCM]_i < 4$ g/m^3. As the *Hyphomicrobium spp* were (re)isolated from BT previously operated with DCM, the observed short adaptation time (8 days) is considered reasonable. Hinojosa-Reyes et al. (2012) reported a start-up period time of 39 days during the biological treatment of ethylbenzene.

During phase II, the tests were performed with Q_{gas} of 0.06 m^3/h ($\tau = 120$ s), $[DCM]_i$ and an ILR in the range of 4–5 g/m^3 and 120.2–150.2 $g/m^3.h$, respectively. During this stage, the steady-state $\%DCM_r$ and EC ranged from 93.9 % to 98.6 % and 120.2 $g/m^3.h$ to 148.0 $g/m^3.h$, respectively. Significant $\%DCM_r$ and EC were maintained throughout the tests at higher $[DCM]_i$ and Q_{gas}. As will be examined further, phase III was meant to combine the APHR with the CSTBR and will be discussed in the next section. Phase IV was characterized by its short residence time and high DCM loading rates. The CSTBR was operated at a Q_{gas} of 0.12 m^3/h ($\tau = 60$ s), $[DCM]_i$ and an ILR in the range of 1–12.6 g/m^3 and 60.3–760 $g/m^3.h$, respectively. The results showed a maximum $\%DCM_r$ and EC of 99.9 % and 546 $g/m^3.h$, respectively. Following that, in phase V, a high $\%DCM_r$ of 100 % (EC ~396 $g/m^3.h$) was achieved at higher Q_{gas} of 0.24 m^3/h, $[DCM]_i$ of 12.4 g/m^3, and ILR of 740.3 $g/m^3.h$. In all the aforementioned phases of operation, an instantaneous decrease in the reported $\%DCM_r$ was observed after each increase in the DCM loading, which was significant during operation under short τ, due to insufficient contact time between the gas and the microorganisms. However, the recovery of the CSTRB was very fast, usually within 3–9 h. The EC values reported in the present study are comparable or higher than the values reported for other VOCs. Almomani et al. (2018) reported a maximum EC and $\%DCM_r$ of 160 $mg/m^3.h$ and 22 % ± 4% under an ILR of 200 $mg/m^3.h$. Hinojosa-Reyes et al. (2012) showed an average EC for ethylbenzene of 45 $g/m^3.h$ (removal of 45 %) at an ILR of 127 ± 9.8 $g/m^3.h$. Kwon and Cho (2009) and Zhu et al. (1998) achieved ECs between 86 and 23 $g/m^3.h$ during the biofiltration of BTEX using cork and granular activated carbon (GAC). Hartmans and Tramper (1991) and Okkerse et al. (1999) demonstrated a $\%DCM_r$ of 30 % at low DCM loading rates. These studies concluded limited DCM removal efficiency during BT.

Fig. 5b presents the evolution of the EC as a function of the ILR of DCM. There was a discernible increase in the EC as the ILR was increased from 16 to 260 $g/m^3.h$, suggesting excellent degradation rate of DCM at the assigned τ. The results showed a high EC (> 200 $g/m^3.h$) for ILR up to 260 $g/m^3.h$ at a Q_{gas} of 0.06 m^3/h ($\tau = 2$ min). However, as the ILR was increased to values > 260 $g/m^3.h$, at higher flow rate (> 0.12 m^3/h) and a shorter $\tau < 1$ min, the EC values dropped to < 200 $g/m^3.h$. As such, it is highly recommended to adjust the Q_{gas} in relation to the $[DCM]_i$, in order to achieve the required EC. For practical applications, uniform Q_{gas} and constant $[DCM]_i$ can only be achieved if a pre-treatment process is installed prior to the CSTBR, as recommended by Amat et al. (2005), Li and Moe (2005), Sano et al. (2004) and Sempere et al. (2010).

Another important factor to monitor the performance of the BT is the biomass concentration in the CSTBR, which does not appear to be a factor in lowering the $\%DCM_r$ in all of the tested phases of bioreactor

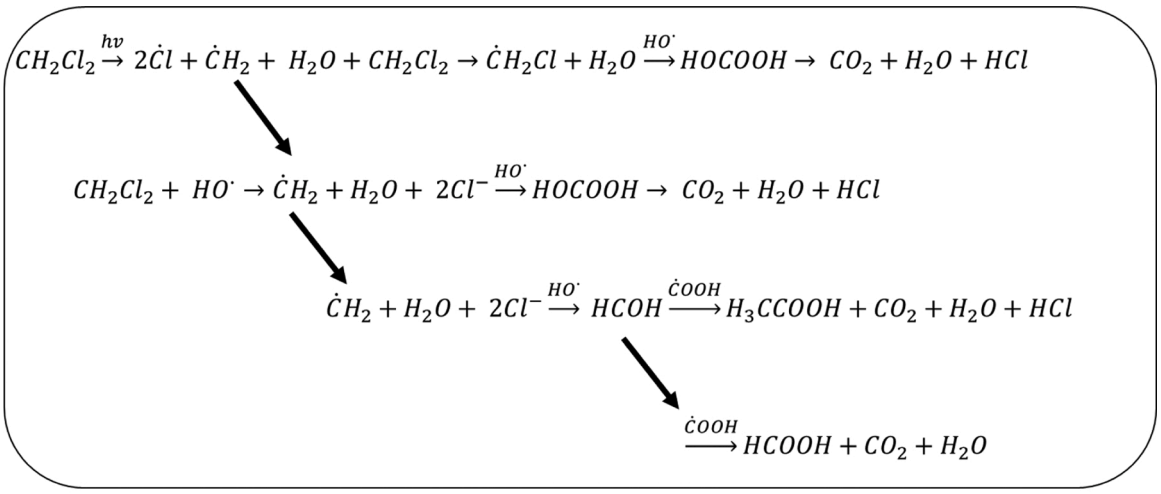

(a)

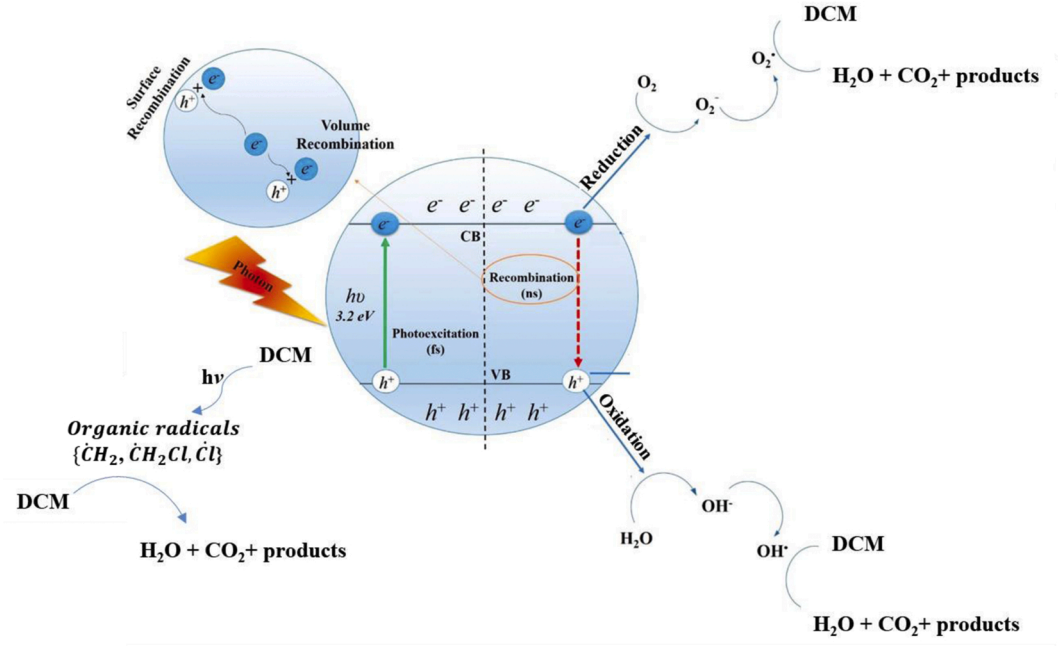

(b)

Fig. 4. (a) The mechanism for DCM oxidation and (b) Surface photo-excitation TiO_2 reactions.

Table 3
The operational schedule of the CSTB in treating gas phase DCM.

Stage	Operating time, d	Q, (m^3/h)	$[DCM]_i$ g/m^3	%DCM_r			ILR, (g/m^3·h)			EC, (g/m^3·h)		
				Average	Max	Min	Average	Max	Min	Average	Max	Min
I	1 – 28	0.12	0.27 – 4.00	85.33	99.6	24.5	154.0	240	16.3	137.8	234	4.00
II	29 – 38	0.06	4.00 – 5.00	96.65	98.6	93.9	143.3	150.2	138.5	148	120.2	116.0
III	39 – 67											
IV	68 – 117	0.12	1.00 – 12.60	78.28	99.9	54.2	501.3	760	60.3	372.8	546	60.0
V	118 – 232	0.24	0.17 – 12.40	69.28	100.0	32.4	332.1	740.3	20.4	195.8	396.0	20.8

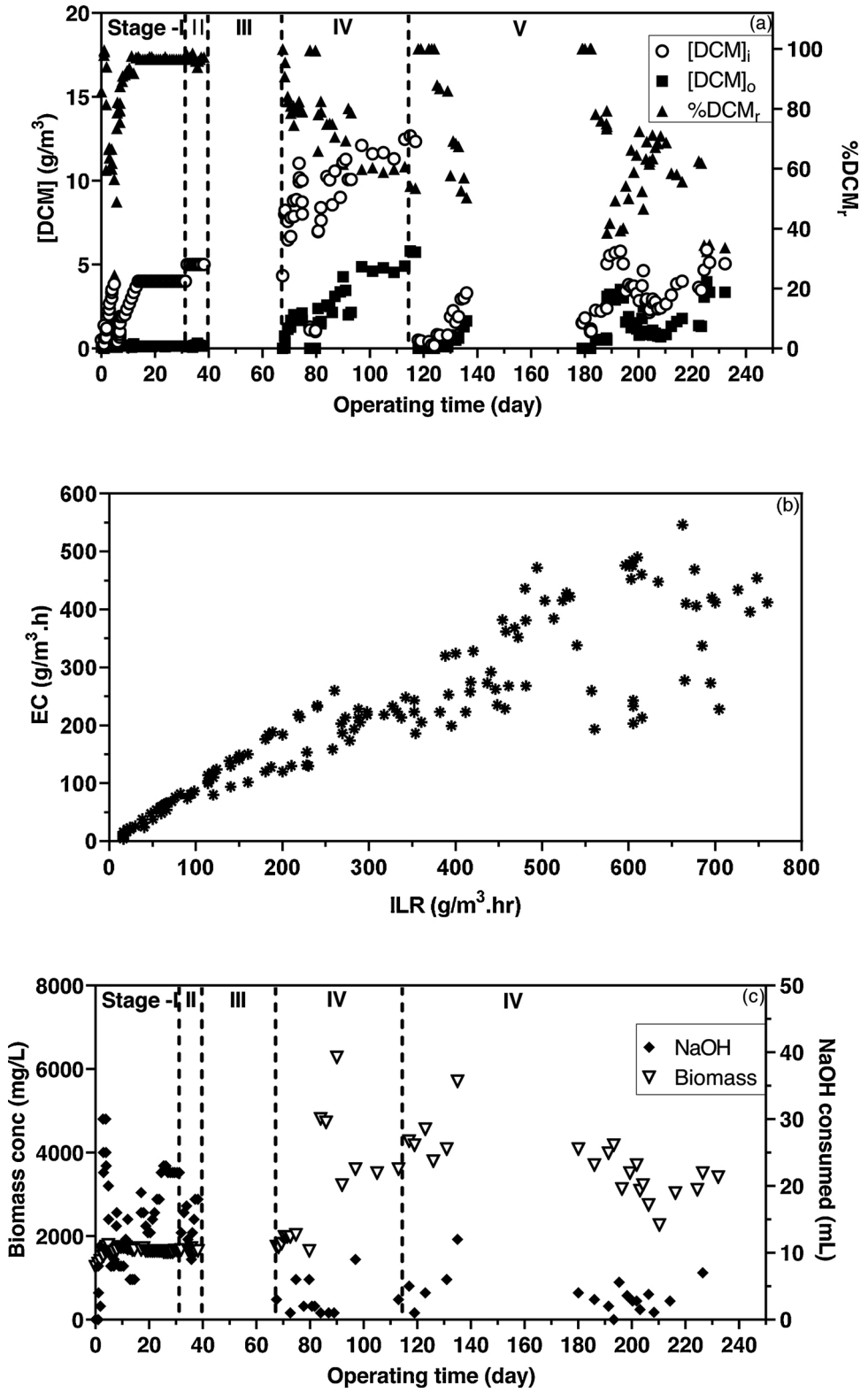

Fig. 5. (a) Profile of inlet, outlet DCM and %DCM_r during the operation of the CSTBR, (b) evaluation of the EC as a function of inlet loading rate, and (c) evaluation of biomass concentration and NaOH consumption by CSTBR.

operation. It can be seen from Fig. 5c that the biomass concentration is nearly uniform. As the biodegradation of one mole DCM produced two moles of HCl and one mole CO_2 as a final product following reaction (16) (Bailón et al., 2009), a solution of 2 N NaOH was continuously supplied to the CSTBR to control and maintain the pH of the mineral medium. Fig. 5c also shows that the NaOH consumption profile is linearly proportional to the %DCMr.

$$CH_2 - Cl_2 + O_2 \rightarrow CO_2 + 2HCl \quad \text{(Reaction 16)}$$

Following reaction (16), the degree of mineralization of DCM can be correlated to the amount of either CO_2 or HCl produced in the

bioreactor. As the concentration of CO_2 in the CSTBR can be generated from the degradation of DCM and endogenous respiration, the level might not provide an accurate indication of the degradation of DCM. Conversely, the chlorine ion or HCl can only be produced from the biodegradation of DCM and cannot be consumed by microorganisms (Kennes et al., 2009). Therefore it was used to calculate the degree of mineralization of DCM. Following reaction (16), the degradation of one mole of DCM produces two moles of HCl that requires equimolar concentration of NaOH to neutralize it. A mass balance over the CSTBR showed that the degree of mineralization of DCM was in the range of 45%–65%.

3.5. Response of the BT to shock loads

Fig. 6a and b illustrate the evolution of the $[DCM]_i$, $[DCM]_o$, ILR, $\%DCM_r$ and EC profiles during the short term shock load tests. The response of the BT to the short term shock load was fast, as demonstrated by the immediate decrease in $\%DCM_r$ after the sudden increase in the $[DCM]_i$. Both $\%DCM_r$ and EC decreased drastically from > 82 % to 43 % and ~ 250 to < 50 g/m^3·h. The reactor required at least 4.7 h to recover after the end of the shock load. It was observed that, when the concentrations were restored to previous values, the $[DCM]_o$ were higher than the $[DCM]_i$, showing negative $\%DCM_r$. This trend suggests that, during continuous operation of the BT, an immediate switch over of concentration (i.e., from high to low values) requires a certain time for the reactor to re-stabilize. Furthermore, at high Q_{gas} and during the switch over period, a small amount of DCM mixed with the suspended liquid could potentially be stripped off, which would result in higher concentrations at the outlet rather than at the inlet. Different trends were observed in the long-term shock load tests (Figs. 6c and d). Increasing the $[DCM]_i$ from 0.6 to 5.5 g/m^3 led to a gradual drop in the $\%DCM_r$ during the first 5 h of the shock load, and subsequently, the $\%DCM_r$ recovered, to reach $\sim$ 40 % after 6.4 h. However, the EC values remained at $\sim$ 200 g/m^3.h at high $[DCM]_i$ of 5.5 g/m^3, and it decreased to < 15 g/m^3·h when the $[DCM]_i$ was reduced to its pre-shock value of 1 g/m^3. It should be mentioned that during the 232 days of operation of the CSTBR, there was no accumulation of organic matter (COD or BOD_5) in the reaction medium suggesting a complete mineralization of the organic matter. The observed trends highlight the sensitivity of the CSTBR and the suspended *Hyphomicrobium spp.* to fluctuations in inlet pollutant concentrations. In addition, the stabilization times of the CSTBR under different operational conditions also had a significant effect on its removal performance. From a practical point of view, a pretreatment or equalization stage is required to guarantee stable CSTBR performance.

3.6. Treatment of DCM in the sequential AOPs-BT

Table 2 presents a summary of the results achieved by combining the AOPs with the BT. These tests were carried out at different $[DCM]_i$, Q_{gas} and τ. Although the UV process was ineffective in degrading and removing DCM from the gas stream (maximum $\%DCM_r < 10$ %), the combined UV-BT processes reached a high $\%DCM_r$ in the range of 14.25 %–98.9 %, with the highest removals observed for tests carried out at $[DCM]_i < 0.45$ g/m^3. The tests performed with $[DCM]_i$ in the range of 0.45 g/m^3 to 4.5 g/m^3 exhibited a maximum $\%DCM_r$ of 22.5 %. The improvement in DCM removal in the sequential UV-BT may be related to the efficiency of both the APHR and the BT in removing DCM at low concentrations. The UV-TiO_2-BT processes exhibited a significant $\%DCM_r$ in the range of 96.6 %–99.7 % under all the tested concentrations. The high $\%DCM_r$ achieved in this process can be attributed to the effective degradation of DCM by UV-TiO_2, as well as the BT.

4. Conclusions

The treatment of a WG stream contaminated with DCM was investigated in a UV, UV-TiO_2, BT reactor and their combination (UV-BT or UV-TiO_2-BT). The effect of process variables, including Q_{gas}, $[DCM]_i$, τ, %RH and PH-C_L on the process performance was determined. The CCD-SA was employed to identify the optimum operating conditions to achieve steady-state DCM removal. The low removal efficiency of the UV photolysis process (≤ 10 %) was enhanced to 70 % by adding 5 g/m^2 of TiO_2 as the photocatalyst. The photocatalytic process was characterized by the production of highly reactive radicals converting DCM to soluble

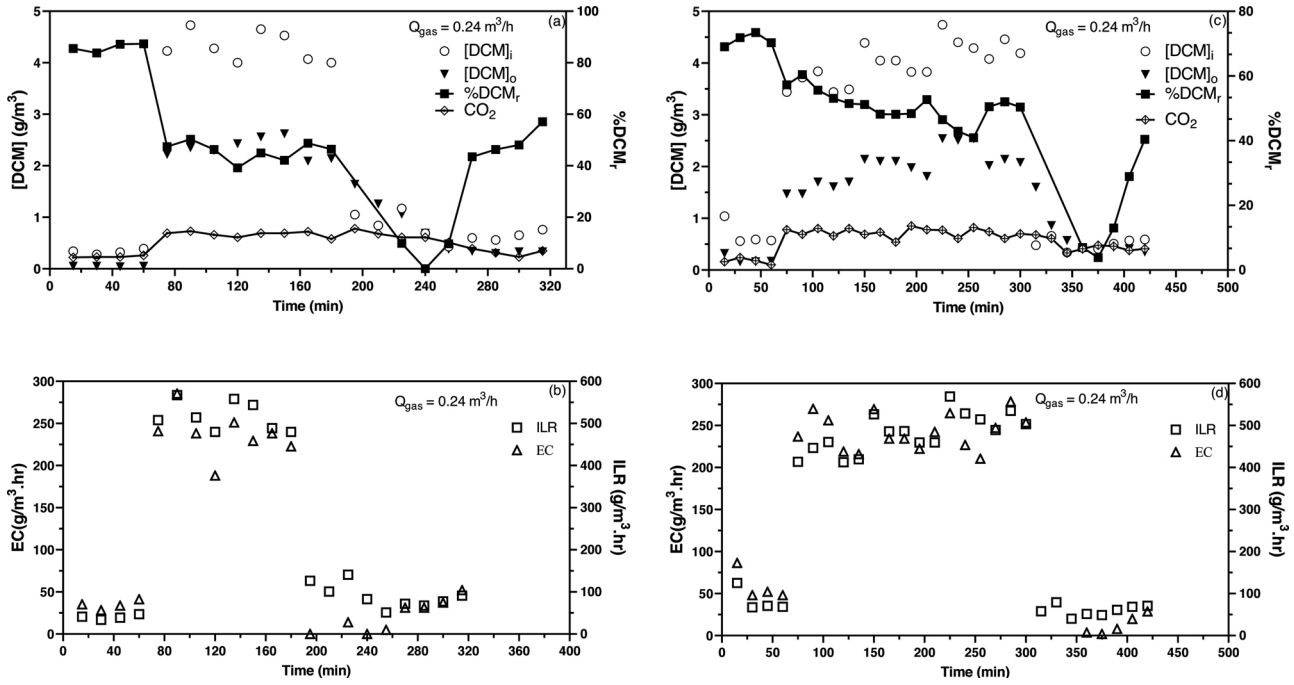

Fig. 6. (a) Evolution of inlet and outlet concentration of DCM, $\%DCM_r$ and CO_2 production as a function of operating time during short-term shock load (b) The EC and ILR as a function of time during short-term shock load (c) The evolution of inlet and outlet concentrations of DCM, $\%DCM_r$, and CO_2 production as a function of operating time during long-term shock load and, (d) The EC and ILR as a function of time during the long-term shock load.

by-products that can be washed out with water and subsequently mineralized in an inexpensive and simple BT. The performance of the oxidation processes decreased at higher Q_{gas} and $[DCM]_i$, and shorter τ, though it was able to improve by increasing the %RH up to 50 %. The combined AOPs-BT achieved high (≥ 95.5 %) DCM removal within a short amount of time. Additionally, the AOP contributed to DCM degradation, acted as a load equalization system, and reduced pollutant load fluctuations during periodic shock loads.

CRediT authorship contribution statement

Fares Almomani: Conceptualization, Methodology, Software, Validation, Writing - review & editing. **Eldon R. Rene:** Writing - original draft, Data curation. **María C. Veiga:** Data curation, Validation. **Rahul R. Bhosale:** Software, Validation, Writing - review & editing. **Christian Kennes:** Conceptualization, Methodology, Writing - review & editing.

Declaration of Competing Interest

The authors report no declarations of interest.

Acknowledgments

The BIOENGIN group at University of La Coruña thanks the Xunta de Galicia for its financial support to Competitive Reference Research Groups (GRC) (ED431C 2017/66). ERR thanks IHE Delft (The Netherlands) for providing infrastructural and "staff time" support. Open Access funding provided by the Qatar National Library.

References

Al Momani, F., 2007a. Degradation of cyanobacteria anatoxin-a by advanced oxidation processes. Sep. Purif. Technol. 57, 85–93.
Al Momani, F., 2007b. Treatment of air containing volatile organic carbon: elimination and post treatment. Environ. Eng. Sci. 24, 1038–1047.
Al Momani, F., Jarrah, N., 2009. Solar/UV-induced photocatalytic degradation of volatile toluene. Environ. Technol. 30, 1085–1093.
Al Momani, F.A., Jarrah, N., 2010. Treatment and kinetic study of cyanobacterial toxin by ozone. J. Environ. Sci. Health 45, 719–731.
Al Momani, F., Gonzalez, O., Sans, C., Esplugas, S., 2004. Combining photo-Fenton process with biological sequencing batch reactor for 2,4-dichlorophenol degradation. Water Sci. Technol. 49, 293–298.
Almomani, F., Bhosale, R., Kumar, A., Kennes, C., 2016a. Removal of volatile sulfur compounds by solar advanced oxidation technologies and bioprocesses. Sol. Energy 135, 348–358.
Almomani, F.A., Shawaqfah, M., Bhosale, R.R., Kumar, A., 2016b. Removal of emerging pharmaceuticals from wastewater by ozone-based advanced oxidation processes. Environ. Prog. Sustain. Energy 35, 982–995.
Almomani, F.A., Bhosale, R.R., Khraisheh, M.A.M.M., Kumar, A., Kennes, C., 2018. Mineralization of dichloromethane using solar-oxidation and activated TiO_2: pilot scale study. Sol. Energy 172, 116–127.
Almomani, F., Bhosale, R., Shawaqfah, M., 2020. Solar oxidation of toluene over Co doped nano-catalyst. Chemosphere, 126878.
Amat, A.M., Arques, A., Lopez, F., Miranda, M.A., 2005. Solar photo-catalysis to remove paper mill wastewater pollutants. Sol. Energy 79, 393–401.
Amoah-Antwi, C., Kwiatkowska-Malina, J., Thornton, S.F., Fenton, O., Malina, G., Szara, E., 2020. Restoration of soil quality using biochar and brown coal waste: A review. Sci. Total Environ. 722, 137852.
APHA, 1985. WPCF, Standard Methods for the Examination of Water and Wastewater. American Public Health Association.
Bailón, L., Nikolausz, M., Kästner, M., Veiga, M.C., Kennes, C., 2009. Removal of dichloromethane from waste gases in one-and two-liquid-phase stirred tank bioreactors and biotrickling filters. Water Res. 43, 11–20.
Beauchet, R., Magnoux, P., Mijoin, J., 2007. Catalytic oxidation of volatile organic compounds (VOCs) mixture (isopropanol/o-xylene) on zeolite catalysts. Catal. Today 124, 118–123.
Blanco, J., Malato, S., Fernández, P., Vidal, A., Morales, A., Trincado, P., et al., 1999. Compound parabolic concentrator technology development to commercial solar detoxification applications. Sol. Energy 67, 317–330.
Bravo, D., Ferrero, P., Penya-roja, J.M., Álvarez-Hornos, F.J., Gabaldón, C., 2017. Control of VOCs from printing press air emissions by anaerobic bioscrubber: Performance and microbial community of an on-site pilot unit. J. Environ. Manage. 197, 287–295.
Chen, J.-M., Chen, Z.-W., Jiang, Y.-F., Zhang, L.-L., 2010. Direct VUV photodegradation of gaseous α-pinene in a spiral quartz reactor: intermediates, mechanism, and toxicity/biodegradability assessment. Chemosphere 81, 1053–1060.
Chen, W.-H., Chen, Z.-B., Yuan, C.-S., Hung, C.-H., Ning, S.-K., 2016. Investigating the differences between receptor and dispersion modeling for concentration prediction and health risk assessment of volatile organic compounds from petrochemical industrial complexes. J. Environ. Manage. 166, 440–449.
Cheng, Z.-W., Jiang, Y.-F., Zhang, L.-L., Chen, J.-M., Wei, Y.-Y., 2011. Conversion characteristics and kinetic analysis of gaseous α-pinene degraded by a VUV light in various reaction media. Sep. Purif. Technol. 77, 26–32.
Cheng, Z., Li, C., Chen, D., Chen, J., Zhang, S., Ye, J., et al., 2019. A novel array of double dielectric barrier discharge combined with TiCo catalyst to remove high-flow-rate toluene: Performance evaluation and mechanism analysis. Sci. Total Environ. 692, 940–951.
Chlala, D., Labaki, M., Giraudon, J.-M., Gardoll, O., Denicourt-Nowicki, A., Roucoux, A., et al., 2016. Toluene total oxidation over Pd and Au nanoparticles supported on hydroxyapatite. Comptes Rendus Chim. 19, 525–537.
Contreras, S., Rodrıguez, M., Al Momani, F., Sans, C., Esplugas, S., 2003. Contribution of the ozonation pre-treatment to the biodegradation of aqueous solutions of 2, 4-dichlorophenol. Water Res. 37, 3164–3171.
Devinny, J.S., Deshusses, M.A., Webster, T.S., 1998. Biofiltration for Air Pollution Control. CRC press.
Diks, R., Ottengraf, S., 1991. Verification studies of a simplified model for the removal of dichloromethane from waste gases using a biological trickling filter. Bioprocess Eng. 6, 93–99.
Directive, 2013. Directive 2013/39/EU of the European Parliament and of the Council of 12 August 2013 Amending Directives 2000/60/EC and 2008/105/EC As Regards Priority Substances in the Field of Water Policy.
Farhanian, D., Haghighat, F., Lee, C.-S., Lakdawala, N., 2013. Impact of design parameters on the performance of ultraviolet photocatalytic oxidation air cleaner. Build. Environ. 66, 148–157.
Feiyan, C., Pehkonen, S.O., Ray, M.B., 2002. Kinetics and mechanisms of UV-photodegradation of chlorinated organics in the gas phase. Water Res. 36, 4203–4214.
Feng, Y., Li, L., Ge, M., Guo, C., Wang, J., Liu, L., 2010. Improved Catalytic Capability of Mesoporous TiO_2 Microspheres and Photodecomposition of Toluene. ACS Appl. Mater. Interfaces 2, 3134–3140.
Feng, Y., Bie, P., Wang, Z., Wang, L., Zhang, J., 2018. Bottom-up anthropogenic dichloromethane emission estimates from China for the period 2005–2016 and predictions of future emissions. Atmos. Environ. 186, 241–247.
Han, Z., Chang, V.-W., Wang, X., Lim, T.-T., Hildemann, L., 2013. Experimental study on visible-light induced photocatalytic oxidation of gaseous formaldehyde by polyester fiber supported photocatalysts. Chem. Eng. J. 218, 9–18.
Han, M.-F., Wang, C., Fu, Y., 2018. Treatment of hydrophobic volatile organic compounds using two-liquid phase biofilters. Sci. Total Environ. 640-641, 1447–1454.
Hartmans, S., Tramper, J., 1991. Dichloromethane removal from waste gases with a trickle-bed bioreactor. Bioprocess Eng. 6, 83–92.
Hassan, A.A., Sorial, G.A., 2011. Treatment of dynamic mixture of hexane and benzene vapors in a trickle bed air biofilter integrated with cyclic adsorption/desorption beds. Chemosphere 82, 521–528.
Hein, L., White, L., Miles, A., Roberts, P., 2018. Analysing the impacts of air quality policies on ecosystem services; a case study for Telemark, Norway. J. Environ. Manage. 206, 650–663.
Hinojosa-Reyes, M., Rodríguez-González, V., Arriaga, S., 2012. Enhancing ethylbenzene vapors degradation in a hybrid system based on photocatalytic oxidation UV/TiO_2 in and a biofiltration process. J. Hazard. Mater. 209-210, 365–371.
Hisatomi, T., Kubota, J., Domen, K., 2014. Recent advances in semiconductors for photocatalytic and photoelectrochemical water splitting. Chem. Soc. Rev. 43, 7520–7535.
Hoffmann, M.R., Martin, S.T., Choi, W., Bahnemann, D.W., 1995. Environmental applications of semiconductor photocatalysis. Chem. Rev. 95, 69–96.
Kasperczyk, D., Urbaniec, K., Barbusinski, K., Rene, E.R., Colmenares-Quintero, R.F., 2019. Application of a compact trickle-bed bioreactor for the removal of odor and volatile organic compounds emitted from a wastewater treatment plant. J. Environ. Manage. 236, 413–419.
Kennes, C., Veiga, M.C., 2001. Bioreactors for Waste Gas Treatment. Kluwer Academic Publishers/Springer, Dordrecht, The Netherlands.
Kennes, C., Veiga, M.C., 2013. Air Pollution Prevention and Control: Bioreactors and Bioenergy. John Wiley & Sons, Chichester, United Kingdom.
Kennes, C., Rene, E.R., Veiga, M.C., 2009. Bioprocesses for air pollution control. J. Chem. Technol. Biotechnol. 84, 1419–1436.
Keppler, F., Barnes, J.D., Horst, A., Bahlmann, E., Luo, J., Nadalig, T., et al., 2019. Chlorine isotope fractionation of the major chloromethane degradation processes in the environment. Environ. Sci. Technol.
Koh, L.H., Kuhn, D.C., Mohseni, M., Allen, D.G., 2004. Utilizing ultraviolet photooxidation as a pre-treatment of volatile organic compounds upstream of a biological gas cleaning operation. J. Chem. Technol. Biotechnol. 79, 619–625.
Kwon, S.-H., Cho, D., 2009. A comparative, kinetic study on cork and activated carbon biofilters for VOC degradation. J. Ind. Eng. Chem. 15, 129–135.
Lau, T., Chu, W., Graham, N., 2007. Degradation of the endocrine disruptor carbofuran by UV, O_3 and O_3/UV. Water Sci. Technol. 55, 275–280.
Li, C., Moe, W.M., 2005. Activated carbon load equalization of discontinuously generated acetone and toluene mixtures treated by biofiltration. Environ. Sci. Technol. 39, 2349–2356.
Li, H.-Y., Gao, P.-P., Ni, H.-G., 2019. Emission characteristics of parent and halogenated PAHs in simulated municipal solid waste incineration. Sci. Total Environ. 665, 11–17.

Matějová, L., Topka, P., Kaluža, L., Pitkäaho, S., Ojala, S., Gaálová, J., et al., 2013. Total oxidation of dichloromethane and ethanol over ceria-zirconia mixed oxide supported platinum and gold catalysts. Appl. Catal. B 142-143, 54–64.
Moe, W.M., Collins, K.L., Rhodes, J.D., 2007. Activated carbon load equalization of gas-phase toluene: effect of cycle length and fraction of time in loading. Environ. Sci. Technol. 41, 5478–5484.
Mohseni, M., Zhao, J.L., 2006. Coupling ultraviolet photolysis and biofiltration for enhanced degradation of aromatic air pollutants. J. Chem. Technol. Biotechnol. 81, 146–151.
Moussavi, G., Mohseni, M., 2007. Using UV pretreatment to enhance biofiltration of mixtures of aromatic VOCs. J. Hazard. Mater. 144, 59–66.
Muñoz-Batista, M.J., Kubacka, A., Gómez-Cerezo, M.N., Tudela, D., Fernández-García, M., 2013. Sunlight-driven toluene photo-elimination using CeO_2-TiO_2 composite systems: a kinetic study. Appl. Catal. B 140-141, 626–635.
Nabatilan, M.M., Harhad, A., Wolenski, P.R., Moe, W.M., 2010. Activated carbon load equalization of transient concentrations of gas-phase toluene: effect of gas flow rate during pollutant non-loading intervals. Chem. Eng. J. 157, 339–347.
Nogueira, R.F.P., Silva, M.R.A., Trova, A.G., 2005. Influence of the iron source on the solar photo-Fenton degradation of different classes of organic compounds. Sol. Energy 79, 384–392.
Obee, T.N., Hay, S.O., 1997. Effects of moisture and temperature on the photooxidation of ethylene on titania. Environ. Sci. Technol. 31, 2034–2038.
Okkerse, W., Ottengraf, S., Diks, R., Osinga-Kuipers, B., Jacobs, P., 1999. Long term performance of biotrickling filters removing a mixture of volatile organic compounds from an artificial waste gas: dichloromethane and methylmethacrylate. Bioprocess Eng. 20, 49–57.
Pichat, P., 2003. Photocatalytic degradation of pollutants in water and air: basic concepts and applications. Environ. Sci. Pollut. Control Series 77–120.
Pichat, P., Disdier, J., Hoang-Van, C., Mas, D., Goutailler, G., Gaysse, C., 2000. Purification/deodorization of indoor air and gaseous effluents by TiO_2 photocatalysis. Catal. Today 63, 363–369.
Ravi, R., Philip, L., Swaminathan, T., 2010. Comparison of biological reactors (biofilter, biotrickling filter and modified RBC) for treating dichloromethane vapors. J. Chem. Technol. Biotechnol. 85, 634–639.
Rene, E.R., Al Momani, F., Veiga, M.C., Kennes, C., 2011. Removal of dichloromethane vapours in an integrated bioreactor–photoreactor. Proceedings of the 4th International Conference on Biotechniques for Air Pollution Control and Bioenergy 205–209.
Ribeiro, A.R., Nunes, O.C., Pereira, M.F., Silva, A.M., 2015. An overview on the advanced oxidation processes applied for the treatment of water pollutants defined in the recently launched Directive 2013/39/EU. Environ. Int. 75, 33–51.
Sánchez, B., Cardona, A.I., Romero, M., Avila, P., Bahamonde, A., 1999. Influence of temperature on gas-phase photo-assisted mineralization of TCE using tubular and monolithic catalysts. Catal. Today 54, 369–377.
Sano, T., Negishi, N., Takeuchi, K., Matsuzawa, S., 2004. Degradation of toluene and acetaldehyde with Pt-loaded TiO_2 catalyst and parabolic trough concentrator. Sol. Energy 77, 543–552.
Sempere, F., Martínez-Soria, V., Penya-roja, J.M., Izquierdo, M., Palau, J., Gabaldón, C., 2010. Comparison between laboratory and pilot biotrickling filtration of air emissions from painting and wood finishing. J. Chem. Technol. Biotechnol. 85, 364–370.
Song, D., Wang, Y., Wang, Y., Jiao, L., Yuan, H., 2008. Preparation and characterization of novel structure Co-B hydrogen storage alloy. Electrochem. commun. 10, 1486–1489.
Trevisan, V., Olivo, A., Pinna, F., Signoretto, M., Vindigni, F., Cerrato, G., et al., 2014. CN/TiO_2 photocatalysts: effect of co-doping on the catalytic performance under visible light. Appl. Catal. B 160, 152–160.
Tseng, T.K., Lin, Y.S., Chen, Y.J., Chu, H., 2010. A review of photocatalysts prepared by sol-gel method for VOCs removal. Int. J. Mol. Sci. 11, 2336–2361.
Weber, F.J., Hartmans, S., 1995. Use of activated carbon as a buffer in biofiltration of waste gases with fluctuating concentrations of toluene. Appl. Microbiol. Biotechnol. 43, 365–369.
Wei, Z., Sun, J., Xie, Z., Liang, M., Chen, S., 2010. Removal of gaseous toluene by the combination of photocatalytic oxidation under complex light irradiation of UV and visible light and biological process. J. Hazard. Mater. 177, 814–821.
Yang, L., Liu, Z., Shi, J., Zhang, Y., Hu, H., Shangguan, W., 2007. Degradation of indoor gaseous formaldehyde by hybrid VUV and TiO_2/UV processes. Sep. Purif. Technol. 54, 204–211.
Yang, J., Wang, D., Han, H., Li, C., 2013. Roles of cocatalysts in photocatalysis and photoelectrocatalysis. Acc. Chem. Res. 46, 1900–1909.
Yang, F., Li, Y., Han, Y., Qian, W., Li, G., Luo, W., 2019. Performance of mature compost to control gaseous emissions in kitchen waste composting. Sci. Total Environ. 657, 262–269.
Zhang, G., Xiong, Q., Xu, W., Guo, S., 2014. Synthesis of bicrystalline TiO_2 supported sepiolite fibers and their photocatalytic activity for degradation of gaseous formaldehyde. Appl. Clay Sci. 102, 231–237.
Zhong, L., Su, F.-C., Batterman, S., 2017. Volatile organic compounds (VOCs) in conventional and high performance school buildings in the U.S. Int. J. Environ. Res. Public Health 14, 100.
Zhu, L., Abumaizar, R.J., Kocher, W.M., 1998. Biofiltration of benzene contaminated air streams using compost-activated carbon filter media. Environ. Prog. 17, 168–172.
Zi, W., Chen, Y., Pan, Y., Zhang, Y., He, Y., Wang, Q., 2019. Pyrolysis, morphology and microwave absorption properties of tobacco stem materials. Sci. Total Environ. 683, 341–350.